Journal of
Medical Chemistry

Article

Structure-Based Design of Selective #-Site Amyloid Precursor Protein Cleaving Enzyme 1 (BACE1) Inhibitors: Targeting the Flap to Gain Selectivity over BACE2

Kazuki Fujimoto, Eriko Matsuoka, Naoya Asada, Genta Tadano, Takahiko Yamamoto, Kenji Nakahara, Kouki Fuchino, Hisanori Ito, Naoki Kanegawa, Diederik Moechars, Harrie J.M. Gijsen, and Ken-ichi Kusakabe

J. Med. Chem., **Just Accepted Manuscript** • DOI: 10.1021/acs.jmedchem.9b00309 • Publication Date (Web): 25 Apr 2019

ACS Publications

is published by the American Chemical Society. 1155 Sixteenth Street N.W., Washington, DC 20036

Structure-Based Design of Selective β-Site Amyloid Precursor Protein Cleaving Enzyme 1 (BACE1) Inhibitors: Targeting the Flap to Gain Selectivity over BACE2

Kazuki Fujimoto,[†,#] *Eriko Matsuoka,*[†,#] *Naoya Asada,*[†,#] *Genta Tadano,*[†,#] *Takahiko Yamamoto,*[†,⊥] *Kenji Nakahara,*[†] *Kouki Fuchino,*[†] *Hisanori Ito,*[†] *Naoki Kanegawa,*[‡] *Diederik Moechars,*[∥] *Harrie J.M. Gijsen,*[§] *and Ken-ichi Kusakabe*[*,†]

[†]Discovery Research Laboratory for Core Therapeutic Areas, [‡]Research Laboratory for Development, Shionogi Pharmaceutical Research Center, 1-1 Futaba-cho 3-chome, Toyonaka, Osaka 561-0825, Japan

[§]Medicinal Chemistry, [∥]Neuroscience Biology, Janssen Research & Development, Turnhoutseweg 30, B-2340 Beerse, Belgium

ABSTRACT

BACE1 inhibitors hold potential as agents in disease-modifying treatment for Alzheimer's disease. BACE2 cleaves the melanocyte protein PMEL in pigment cells of the skin and eye, generating melanin pigments. This role of BACE2 implies that non-selective and chronic inhibition of BACE1 may cause side effects derived from BACE2. Herein, we describe the discovery of potent and selective BACE1 inhibitors using structure-based drug design. We targeted the flap region, where the shape and flexibility differ between these enzymes. Analysis of the cocrystal structures of an initial lead **8** prompted us to incorporate spirocycles followed by its fine-tuning, culminating in highly selective compounds **22**. The structures of **22** bound to BACE1 and BACE2 revealed that a relatively high energetic penalty in the flap of the **22**-bound BACE2 structure may cause a loss in BACE2 potency, thereby leading to its high selectivity. These findings and insights should contribute to responding to the challenges in exploring selective BACE1 inhibitors.

INTRODUCTION

Alzheimer's disease (AD) is the most common form of dementia. In 2016, an estimated 47 million people were living with dementia.[1] Of them, 60 to 80% were estimated to have AD, and 10% of people aged 65 and older were suffering from the disease.[2] The number of patients with AD will escalate rapidly, as the figure is expected to double every 20 years to reach 131 million by 2050.[1] AD ultimately leads to death within 3 to 9 years after diagnosis and is the sixth-leading cause of death in the United States.[2] Additionally, there is a huge impact on the quality of life for both the AD patients and their family caregivers.[1,2] The current therapeutic agents, such as the acetylcholinesterase inhibitors and the *N*-methyl-D-aspartate receptor antagonist, only possess modest symptomatic effects and do not halt or slow the disease progression. Also, the treatment gains obtained from the drugs are often lost within a few years. Therefore, there is a great unmet medical need for a disease-modifying drug that can benefit patients and caregivers by improving clinical outcomes.[3]

The accumulation of extracellular deposits of amyloid plaques composed of amyloid β-peptides (Aβ) with 38 to 43 amino acids is a hallmark of AD. Histopathological and genetic evidence underlie the amyloid cascade hypothesis that AD may be caused by deposition of Aβ.[4] The β-site amyloid precursor protein cleaving enzyme 1 (BACE1), also known as β-secretase, initiates the production of Aβ and hence is a prime target for AD.[5] Since the discovery of BACE1 in 1999,[6] the pharmaceutical industry and academia have pursued orally available and brain penetrant BACE1 inhibitors with an acceptable safety profile. The initially reported BACE1 inhibitors, such as peptidomimetics and hydroxyethylamines, struggled to achieve balanced *in vitro* potency and favorable pharmacokinetic profiles, due to their large molecular weight and high polar surface area.[7] The identification of small molecule amidine-based inhibitors addressed the issues observed in the peptidomimetic analogs.[8,9] Leveraging structure-based design and tuning physicochemical properties culminated in the discovery of several clinical BACE1 inhibitors, such as verubecestat (**1**, MK-8931),[10] elenbecestat (**2**, E-2609),[11] lanabecestat (**3**, AZ-3293),[12] umibecestat (CNP520),[13] and atabecestat (JNJ-

54861911).[14] Unfortunetaly, **1** and **3** failed due to lack of efficacy in their phase III clinical trials,[10d,12b] and the development of atabecestat was stopped due to significant elevation of liver enzymes.[14b]

Chart 1. Representative BACE1 inhibitors in Clinical Development

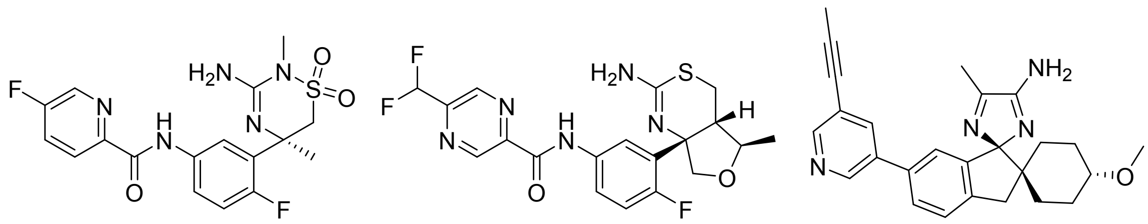

1 (verubecestat) **2** (elenbecestat) **3** (lanabecestat)

The Dominantly Inherited Alzheimer Network (DIAN) study, which enrolled participants at risk for carrying a mutation for autosomal dominant AD, reveals that deposition of Aβ, measured by positron-emission tomography (PET), begins approximately 15 years before the age of expected symptom onset, followed by increased tau protein in the CSF and hippocampal atrophy leading to cognitive and clinical changes.[15] As in the DIAN study, a similar trend of Aβ deposition, brain atrophy, and cognitive decline is observed in patients with sporadic AD.[16] Large phase III studies for **1** and anti-Aβ antibodies involving patients with prodromal or mild-to-moderate AD failed due to no improvement in clinical outcomes,[17] however, this may have been due to the intervention with these anti-Aβ therapies being too late to change the clinical outcomes. Thus, the evidence indicates that anti-Aβ drugs such as BACE1 inhibitors need to be given in the early stage of the disease, most likely at the presymptomatic stages, to prevent the development of AD.[18] This consideration points to the need for chronic administration for more than 20 years, thereby requiring safer profiles for these anti-Aβ drugs including BACE1 inhibitors.

BACE2 is a close homolog of BACE1 (52% sequence identity and 68% sequence similarity) and is primarily expressed in the peripheral tissues but at low levels in the brain.[19] The enzyme cleaves the proproliferative type 1 transmembrane protein TMEM27 involved in the regulation of β cell mass.[20] BACE2 was also found to process the pigment cell-specific melanocyte protein (PMEL), which is specifically expressed in pigment cells of the eye and skin. Indeed, BACE2$^{-/-}$ mice exhibited a silvery depigmented coat.[21] Furthermore, chronic administration of BACE1 inhibitors, such as **1** or NB-360,[9i] resulted in depigmentation of the coats of rats and rabbits.[10b,22] These findings for BACE2 may indicate its potential safety risk associated with chronic and non-selective inhibition of BACE1 inhibitors.

Development of selective BACE1 inhibitors remains a significant challenge, given the homology between BACE1 and BACE2. Indeed, the clinical compounds **1**, **2**, and **3** have suboptimal BACE1 selectivity of 1.0-, 12- and 3.1-fold over BACE2 in our FRET biochemical assay. Although a number of crystal structures of inhibitor-bound BACE1 have been reported,[7b] only a few high-resolution crystal structures are available for BACE2.[23] Bernard and Gsell et al. paved the way to obtaining high quality inhibitor-bound BACE2 structures by the use of surface mutagenesis or crystallization helpers such as camelid heavy chain antibody (also known as V_HH or Nanobody or Xaperone) or human Fyn kinase derived SH3 domain (Fynomer).[23b] Comparative analysis of inhibitor-bound BACE1 and BACE2 structures revealed differences in conformational flexibility in the 10s loop and the flap region, where BACE2 stabilized these closed conformations,[23] whereas BACE1 could accommodate the open conformation.[24] Thus, these conformational differences could make a large binding site available in BACE1 relative to that in BACE2, thereby offering the design strategy of fine-tuning the size of substituents occupying the two sites. At the outset of this work, pioneering work from Wyeth had identified a highly selective inhibitor **4** (Chart 2), where one of the ethyl groups engages with the flap (Chart 3).[25] In parallel with our efforts, several pharmaceutical companies reported selective BACE1 inhibitors, such as compounds **5** (PF-6751979), **6**, and **7**, in patent and scientific literature,[26] which appear to utilize the 10s loop or the flap to gain selectivity, given the crystal structures of the analogues bound to BACE1. Herein, we describe our medicinal chemistry efforts of exploring next generation BACE1 inhibitors with high selectivity over BACE2, starting from Compound J (**8**) (Chart 3).[27] Leveraging the cocrystal structures of **4** and **8** led to a successful strategy of targeting the flap followed by incorporating spirocycles at the 5-position on the thiazine, culminating in the highly selective BACE1 inhibitors **21** and **22**. Comparative analysis of the cocrystal structures of **22** bound to BACE1 and BACE2 provided insight into the selectivity.

Chart 2. Representative Selective BACE1 inhibitors

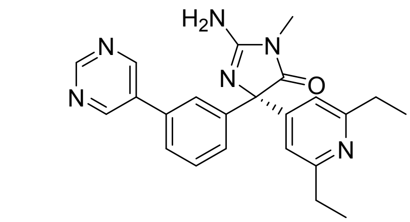

4 (Wyeth)

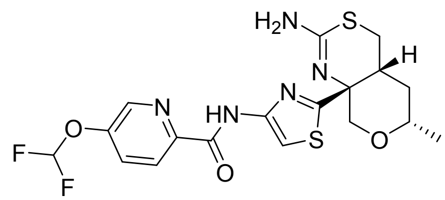

5 (Pfizer)

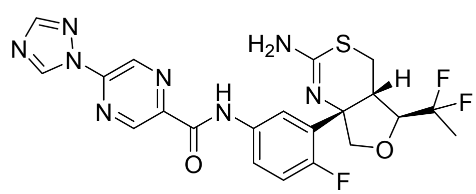

6 (Eli Lilly)

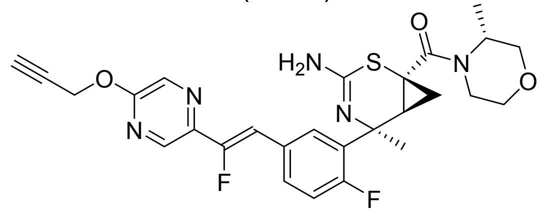

7 (Amgen)

Chart 3. Lead Compounds

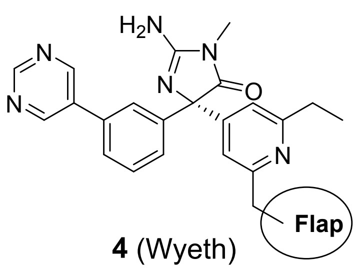

4 (Wyeth)

BACE1 IC_{50}: 44 nM
BACE2 IC_{50}: >10 μM
Selectivity: >227x
Cell Aβ IC_{50}: 138 nM

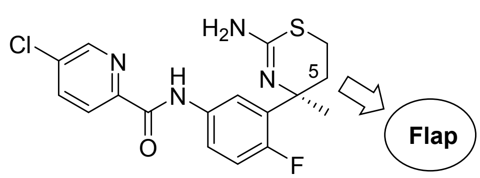

8 (Compound J)

BACE1 IC_{50}: 4.6 nM
BACE2 IC_{50}: 8.7 nM
Selectivity: 1.9x
Cell Aβ IC_{50}: 0.93 nM

RESULTS AND DISCUSSION

Inhibitor Design. As the first step of our efforts, we established the binding mode of compound **8** by soaking it with apo-BACE1 crystals to facilitate medicinal chemistry design.[27] Figure 1A highlighted non-conserved residues around **8**, consisting of key residues of BACE1, such as Pro70, Gln12, and Arg128 located in the flap, 10s loop, and S2' pocket, respectively. At the onset of this study, compound **4**[25] was known as a selective BACE1 inhibitor with a BACE1 selectivity of >227-fold in our FRET biochemical assay (BACE1 IC_{50} = 44 nM, BACE2 IC_{50} = >10 μM), though it suffered from suboptimal cellular potency (IC_{50} = 138 nM; Chart 3). The significant selectivity was rationalized by the favorable interaction of the ethyl group on the pyridine with the flap.[25] Indeed, a difference in the conformation of the flap was observed between BACE1 and BACE2. As mentioned above, the flap in apo BACE1 tends to adopt an open conformation,[24] whereas that in apo BACE2 favors a closed one.[23] Because one of the non-conserved residues in the flap in BACE1 is Pro70, replaced by Lys86 in BACE2, this proline residue may affect the flexibility.[23] Unlike the apo BACE1 structures, the crystal structure of **8** bound to BACE1 adopts a closed conformation in the flap (Figure 1B). Further analysis of the cocrystal structure of **8** suggested that introduction of substituents at the 5-position with the stereochemistry in Figure 1B on the thiazine ring could provide a favorable interaction with Tyr71 in the flap. Therefore, we reasoned that targeting the flap using the cellular potent lead **8** could improve selectivity while retaining cellular potency.

The 10s loop also adopts distinct conformations between BACE1 and BACE2, providing a smaller S3 pocket in BACE2 than in BACE1.[23,24] Thus, utilizing this pocket offers another opportunity to design BACE1 selective inhibitors. Indeed, Hilpert et al. at Roche explored amide substituents in their oxazine series positioned in the S3 pocket.[28] Whereas incorporation of larger substituents at this position achieved increased selectivity, an enzyme-to-cell potency shift was observed in these compounds, resulting in suboptimal cellular activity.[28] With this point in mind, we optimized the amide moiety in **8** interacting with the 10s loop in the S3 pocket, prior to exploring substituents at the 5-positon.

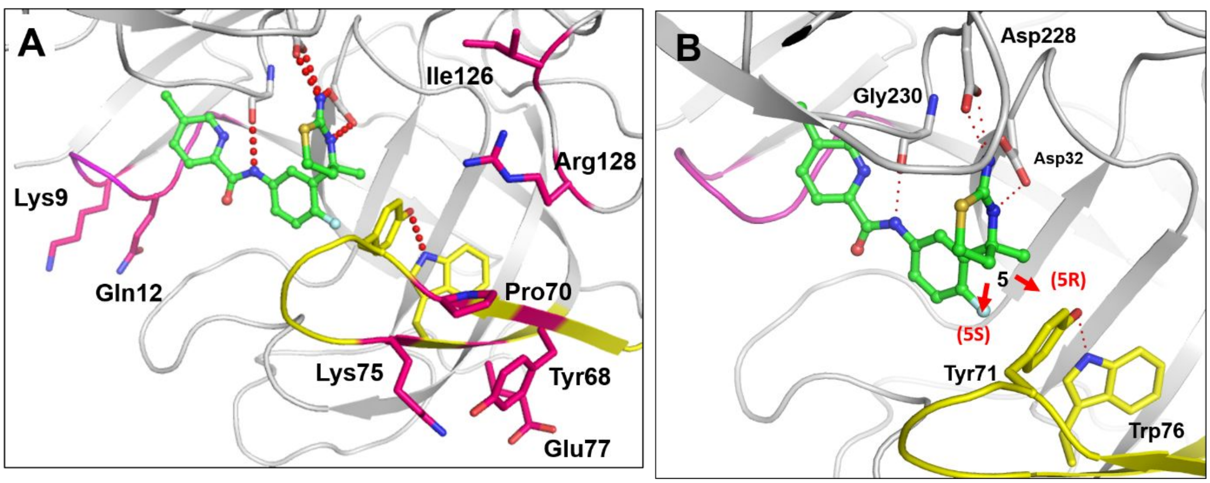

Figure 1. (A) A schematic representation of non-conserved residues between BACE1 and BACE2 including key interactions. (B) Crystal structure of **8** bound to a flap-closed form of BACE1. Substituents projecting from the 5-positon to reach the flap.

Optimization of the Amide Substituent in 8. The optimization began with adjusting the size of the chloro group in **8** to strike a balance between potency and selectivity. Replacement of the chloro with a fluorine (**9**) reduced both BACE1 and BACE2 potency. Compound **10** with a cyano group as a larger substituent had a similar potency to **8** and improved selectivity over BACE2 (6.6-fold). A variety of pyrazine analogs with different R groups (**11-14**) was then pursued. The difluoromethyl **11** displayed a higher BACE2 IC_{50} value of 102 nM, although BACE1 potency was diminished as well. Compound **12**, possessing a methoxy group, imparted an increase in BACE1 potency, whereas the BACE2 activity was retained relative to the difluoro counterpart **11**, resulting in increased BACE1 selectivity. Introduction of a bulkier trifluoromethoxy group (**13**) retained BACE1 activity and, as expected, provided further improvement in selectivity (44-fold). However, as observed in the previous work at Roche,[28] such modification caused an enzyme-to-cell shift, leading to a moderate cellular IC_{50} of 13 nM. A balanced profile of BACE1 selectivity and cellular potency was seen when introducing a fluromethoxy group at the R position, leading to compound **14**. Although the selectivity of **14** was still moderate (16-fold), this compound served as a starting point to explore substituents at the 5-positon on the thiazine ring targeting the flap.

Table 1. Potency and Selectivity of the Amide Analogs

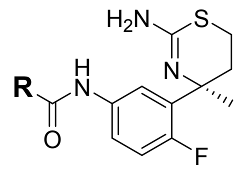

compd	R	Biochemical IC_{50} (nM)[a,b]		Selectivity (BACE2/BACE1)	Cellular Aβ IC_{50} (nM)[a,c]
		BACE1	BACE2		
8	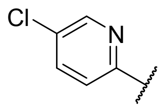	4.6	8.7	1.9x	0.93
9	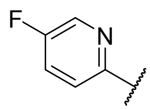	13	14	1.1x	16
10	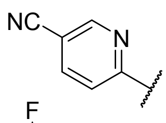	3.2	21	6.6x	0.93
11	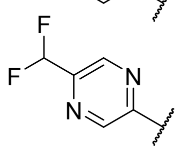	20	102	5.1x	7.2
12	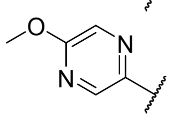	11	85	7.7x	5.4
13	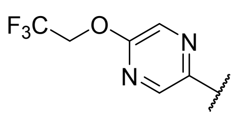	7.2	316	44x	13
14	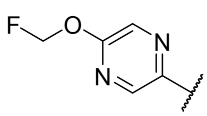	4.9	78	16x	1.8

[a]Values represent the mean values of at least two independent experiments. [b]Biochemical fluorescence resonance energy transfer (FRET) assay. [c]IC_{50} determined by measuring the levels of secreted Aβ42 in a human neuroblastoma SKNBE2 cell line expressing the wild-type amyloid precursor protein (hAPP695) via a sandwich αlisa assay.

Initial Exploration of Substituents at the 5-Position of the Thiazine. As discussed above, the cocrystal structure of **8** in BACE1 prompted the introduction of substituents at the 5-position with the (*R*) configuration as shown in Figure 1B. Addition of a methoxy group provided compound **15**, which reduced BACE2 potency resulting in improved selectivity of 30-fold relative to the non-substituted **14**. The cocrystal structure of the initial lead **8** suggested that larger substituents, such a phenyl group with (*R*)-configuration (**16**), could not be accommodated due to steric hindrance from the flap. To confirm the steric constraint around this region, both (*R*)- and (*S*)-phenyl **16** and **17** were synthesized. Contrary to our expectation, compound **16** increased potency in both BACE1 and BACE2, leading to the same level of selectivity as **14**. The phenyl thiazine **17** with the opposite configuration had a comparable BACE1 potency to **14**, whereas selectivity was decreased due to slightly increased BACE2 activity relative to the (*R*)-phenyl **16**. To gain insight into this unexpected finding, the cocrystal structures of **16** and the diastereomer counterpart **17** bound to BACE1 were solved.

Table 2. Initial Exploration of the 5-Substituted Thiazines

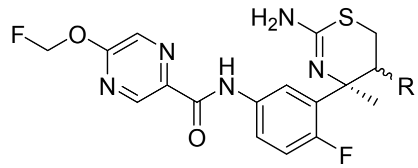

compd	R	Biochemical IC_{50} (nM)[a,b]		Selectivity (BACE2/BACE1)	Cellular Aβ IC_{50} (nM)[a,b]
		BACE1	BACE2		
14	H	4.9	78	16x	1.8
15	(*R*) 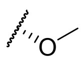	8.3	251	30x	4.5
16	(*R*) 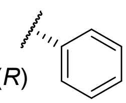	1.7	28	16x	2.3
17	(*S*) 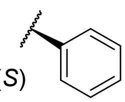	3.3	13	3.9x	2.0

[a]Values represent the mean values of at least two independent experiments. [b]Biochemical fluorescence resonance energy transfer (FRET) assay. [c]IC_{50} determined by measuring the levels of secreted Aβ42 in a human neuroblastoma SKNBE2 cell line expressing the wild-type amyloid precursor protein (hAPP695) via a sandwich αlisa assay.

X-ray Analysis of 16 and 17 Leading to the Design of Spiro-Thiazines. The crystal structure of **16** confirms that the flap adopts an open conformation, unlike that of **8** bound to BACE1 (Figure 2A). The hydrogen bond between the flap residues Tyr71 and Trp76 is disrupted, thereby moving away the Tyr71 side chain to generate a new binding pocket that accomodates the phenyl group in **16**. In contrast, **17** complexed with BACE1 shows a pseudo flap-closed conformation where the side chain in Tyr71 has a good alignment with that of **8**

bound to BACE1 (close conformation), though the hydrogenbond between Tyr71 and Trp76 is not present (a weak water-mediated hydrogen bond is observed), and the phenyl in **17** points toward the solvent region (Figure 2B), explaining why compound **17** exhibited slightly reduced potency in BACE1. We postulated that a similar change may have occurred in BACE2. Therefore, using the cocrystal structure of **16**, we looked for an alternative design of substituents at this position, where the analysis prompted us to incorporate spirocycles that could provide an optimal vector to the flap. Alternatively, replacement of the phenyl in **16** with bulkier substituents, such as saturated rings, was predicted to form favorable interactions with the flap to gain selectivity.

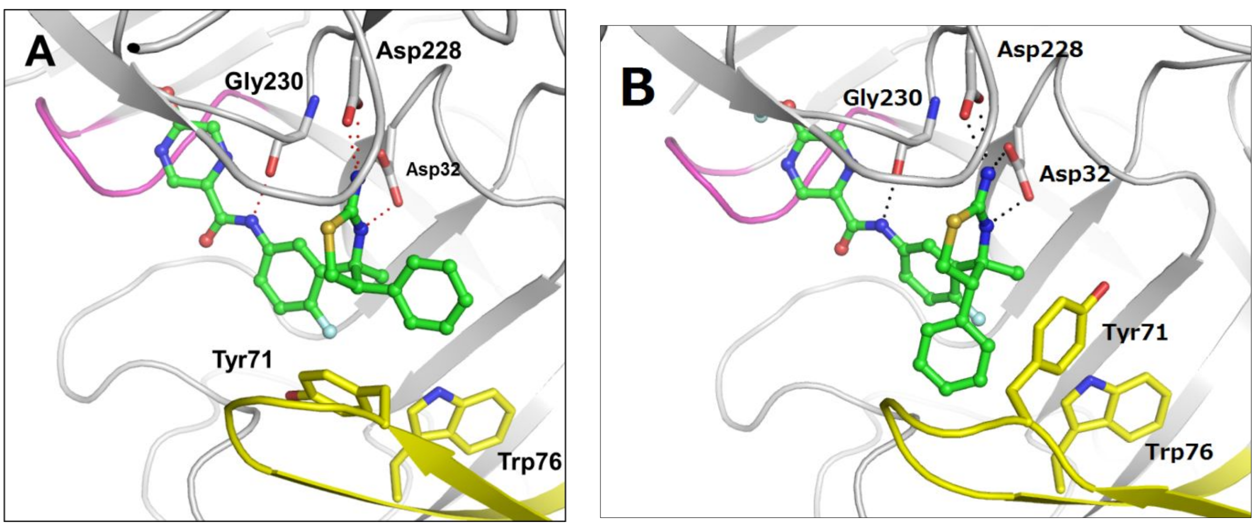

Figure 2. (A) Crystal structure of **16** bound to BACE1. (B) **17** bound to BACE1.

Identification of Selective BACE1 Inhibitors 21 and 22. To test the design hypothesis, a saturated ring of a tetrahydro-2*H*-pyran (**18**) was introduced at the 5-position (Table 3). The compound **18** showed a potency comparable to the phenyl-substituted **16** and improved selectivity over BACE2. To our delight, the corresponding spirocycle **19** provided a further gain in selectivity. The use of a smaller ring size, as in **20**, resulted in a decreased selectivity as expected, whereas compound **21** with a difluorocyclohexyl ring displayed significantly reduced BACE2 potency, achieving a 104-fold selectivity. Further gain in selectivity was realized when the difluoromethylene in **21** was replaced with a sulfonyl group. The sulfonyl compound **22** demonstrated a remarkable 550-fold selectivity in the FRET assay, although this change was associated with reduced cellular potency (Table 3). This result was attributed to low lipophilicity (LogD = 0.62) resulting in a poor permeability of 1.6×10^{-6} cm/s (Table 4). On the other hand, compounds **19** and **21** with good cellular potency displayed improved permeability (Table 4).

Table 3. Optimization of the 5-Substituted Thiazines

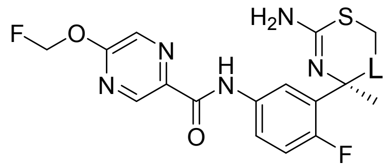

compd	L	Biochemical IC_{50} (nM)[a,b]		Selectivity (BACE2/BACE1)	Cellular Aβ IC_{50} (nM)[a,b]
		BACE1	BACE2		
18	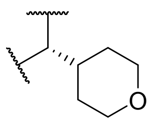	3.2	74	23x	2.0
19	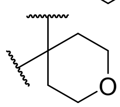	15	631	42x	6.8
20	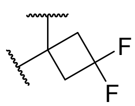	5.5	129	23x	1.2
21	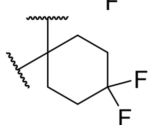	16	1660	104x	4.3
22	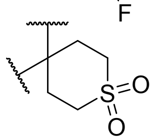	3.8	2090	550x	13

[a]Values represent the mean values of at least two independent experiments. [b]Biochemical fluorescence resonance energy transfer (FRET) assay. [c]IC_{50} determined by measuring the levels of secreted Aβ42 in a human neuroblastoma SKNBE2 cell line expressing the wild-type amyloid precursor protein (hAPP695) via a sandwich αlisa assay.

Table 4. Binding Affinity, Metabolic Stability, P-gp Efflux, and Physicochemical Profiles of 19, 21, and 22

Compd	K_i (nM)[a] BACE1	BACE2	Binding selectivity (BACE2/BACE1)	HLM/MLM[b]	P-gp ER[c]	P_{app}[d]	Log D[e]
19	6.5	479	74x	51 / 5.0	11	21	1.2
21	4.0	2000	500x	27 / 4.5	2.4	7.1	2.3
22	1.9	1740	916x	55 / 17	20	1.6	0.62

[a]The binding affinity (K_i) was determined in a competitive radioligand binding assay using the tritiated non-selective BACE1/BACE 2 inhibitor [^{3}H]-JNJ-962 (JNJ-962: BACE1 K_i = 0.69 nM, BACE2 K_i = 0.29 nM). Values represent the mean values of at least two determinations. [b]% Remaining after 30 min incubation with human liver (HLM) and mouse liver microsomes (MLM). [c]Efflux ratio measured in LLC-PK1 cells transfected with human MDR1. [d]Permeability coefficient measured in LLC-PK1 cells (×10^{-6} cm/s). [k]LogD determined in 1-octanol/phosphate buffer at pH 7.4.

To further investigate the BACE1 selectivity over BACE2 observed in compounds **19**, **21**, and **22**, the binding affinities (K_i) to the respective enzymes were determined in a competitive radio ligand binding assay using a tritiated non-selective BACE1/BACE2 inhibitor (JNJ-962),[29] which had high affinities for both BACE1 and BACE2 (BACE1 K_i = 0.69 nM, BACE2 K_i = 0.29 nM). As shown in Table 4, compound **19** had a binding selectivity of 74-fold, similar to the selectivity observed in the FRET assay. The spiro compounds **21** and **22** achieved a pronounced binding selectivity of 500-fold and 916-fold, respectively. On the basis of the outstanding selectivity observed for **21** and **22**, these compounds were profiled in a mouse pharmacokinetics (PK) and pharmacodynamics (PD) model to investigate their effect on Aβ reduction in the brain.

Prior to the PK/PD study in mouse, metabolic stability and P-gp mediated efflux were profiled including compound **19** (Table 4). Unfortunately, all the compounds exhibited poor metabolic stability in mouse (<20% remaining after 30 min incubation in microsomes), whereas they were more metabolically stable in human. A high P-gp efflux ratio of 20 was realized with the sulfonyl compound **22**, whereas **21**, possessing the difluoromethylene instead of the sulfonyl, showed improved P-gp efflux; the tetrahydropyran **19** also had a high P-gp efflux. This result indicated that polar substituents, such as sulfone and ether moieties, could be involved in an interaction with P-gp, resulting in increased P-gp efflux. Although increasing permeability is often a successful strategy for reducing P-gp efflux, it does not account for the P-gp efflux ratios observed in these compounds.

Mouse PK/PD Study of 21 and 22. Considering the low metabolic stability observed for **21** and **22**, Male ICR (Crlj:CD) mice were orally administered a high dose of 30 mg/kg (n = 4), and the total Aβ levels were measured in the brain at 2, 4, and 6 h post dose. Unfortunately, no significant Aβ reduction was observed for the sulfonyl-substituted **22**. The poor efficacy was explained by the low brain levels at all the time points derived from its low permeability and high P-gp efflux, and consequently it exhibited a brain-to-plasma ratio (K_p) of 0.010. On the other hand, compound **21** with improved P-gp efflux and permeability demonstrated robust Aβ reduction at the same dose (Figure 3). Maximum total Aβ reduction of 61% was observed at 4 h post dose at a brain level of 626 ng/mL with an improved K_p of 0.55. The improved physicochemical properties and reduced P-gp efflux translated into the significantly improved brain levels, which led to the pronounced central activity.

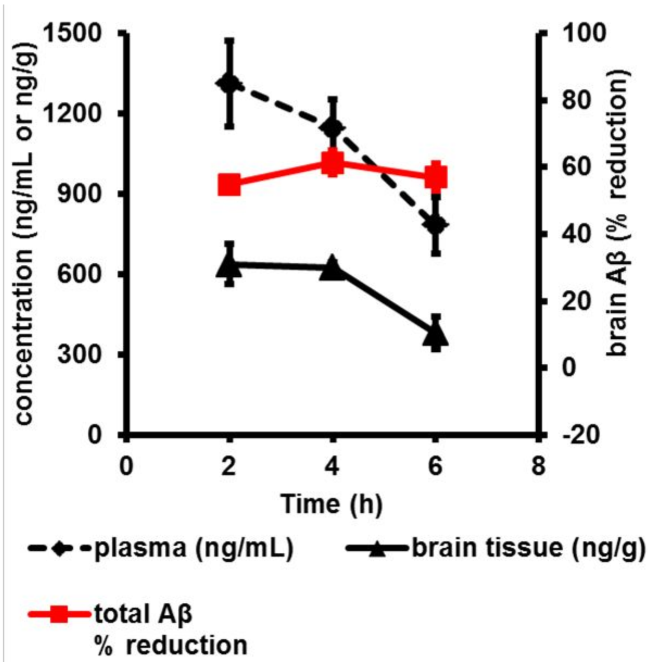

Figure 3. Reduction of total Aβ in the brain of male ICR mice (n = 4) after oral administration of **21** as a solution of 20% 2-hydroxypropyl-β-cyclodextrin (HPBCD) at 30 mg/kg.

Crystal Structures of 22 Bound to BACE1 and BACE2. To gain insight into the pronounced BACE1 selectivity over BACE2 observed in **22**, the cocrystal structures of this compound bound to both the enzymes were determined (Figure 4). Soaking of apo BACE1 crystals generated the **22**-bound BACE1 structure with a resolution of 2.6 Å. Like the **16**-bound BACE1 structure, the flap forms an open conformation, where the hydrogen bond interaction between the phenolic OH in Tyr71 and the indole NH in Trp76 is disrupted

(Figure 4A). A slight movement of the flap over that in apo BACE1 (PDB ID: 1w50)[24a] is observed with a distance of 1.5 Å based on the α carbon in Tyr71 (Figure 4B), whereas no significant movement is seen between the **16**- and **22**-bound BACE1 structures. Unlike the **16**-bound BACE1 structure, the spirocyle in **22** interacts well with the side chain in Tyr71, confirming our design hypothesis.

The binary complex of BACE2 and a crystallization helper of Xaperone XA4813 was cocrystallized with **22** with a resolution of 1.5 Å,[30] according to a paper published from Roche.[23b] As expected, the **22**-bound BACE2 structure displays a flap-open conformation, consistent with the corresponding BACE1 structure (Figure 4C). Notably, the binding of **22** to BACE2 causes a significant movement of the flap by 3.2 Å, relative to its position in an apo BACE2 (PDB ID: 3zkg) (Figure 4D).[23b] Thus, a larger movement of the flap over the apo enzyme is confirmed in the BACE2 (3.2 Å vs 1.5 Å). More importantly, the difference in mean B-factors (temperature factor) between all of the complex and the flap of the **22**-bound BACE2 is up to 18.3 Å^2 (B-factor of the complex = 32.0 Å^2; B-factor of the flap = 50.3 Å^2), whereas in the **22**-bound BACE1, it falls to 2.0 Å^2 (B-factor of the complex = 45.9 Å^2; B-factor of the flap = 47.9 Å^2). This indicates that the **22**-bound BACE2 was destabilized relative to the **22**-bound BACE1, which may result in decreased potency in BACE2 but a retained BACE1 activity, providing an explanation for the increase in selectivity observed in compound **22**. We believe that these structural insights as well as the cocrystal structures of

22 bound to BACE1 and BACE2 could aid the design of novel selective BACE1 inhibitors targeting the flap.

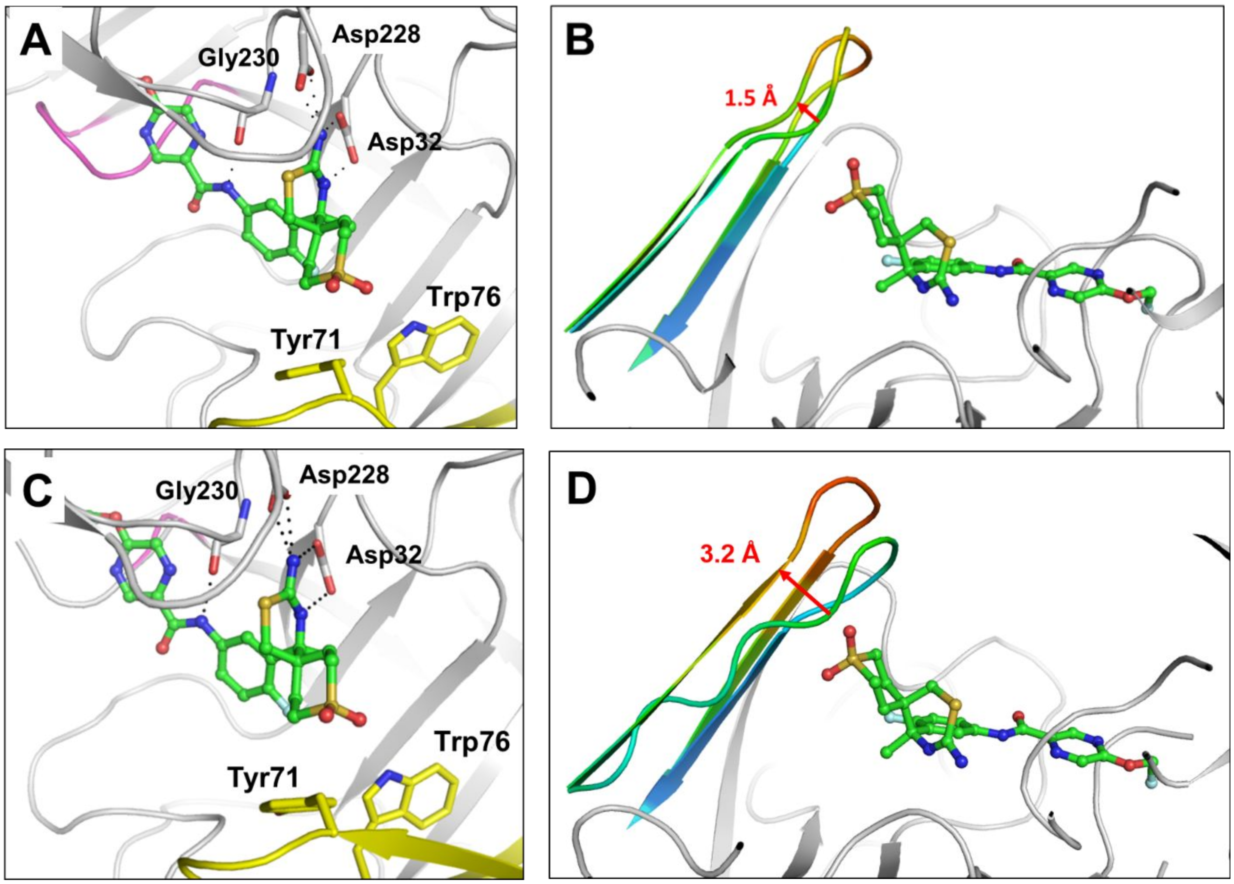

Figure 4. Crystal structure of **22** bound to BACE1 and BACE2. (A) A view of the flap region in the **22**-bound BACE1 structure. (B) Superposition of the flap in the **22**-bound BACE1 and apo BACE1 structure (PDB ID: 1w50). The color in the flap indicates B-factors (Bule: low B-factors; Orange: high B-factors). (C) A view of the flap region in the **22**-bound BACE2 structure. (D) Superposition of the flap in the **22**-bound BACE2 and apo BACE2 structure (PDB ID: 3zkg). The color means the same as B).

CHEMISTRY

The compounds **8–14** bearing various amide moieties were prepared from aniline intermediate **23** (Scheme 1). The aniline **23** and the carboxylic acids used for synthesis of **11**, **13** and **14** were prepared according to known procedures.[27,28,31,32] Amide formation was accomplished without protection of the amidine moiety by adding 1.0 equiv of HCl over **23**, furnishing the thiazines **8–14**.

Scheme 1. Synthesis of Thiazines 8–14[a]

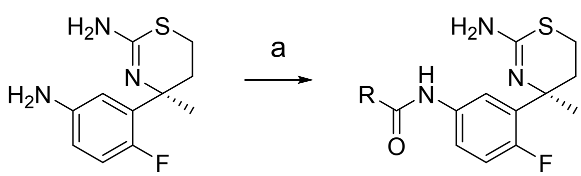

23

8: R = 5-chloro-pyridin-2-yl
9: R = 5-fluoro-pyridine-2-yl
10: R = 5-cyano-pyridine-2-yl
11: R = 5-difluoromethyl-pyrazine-2-yl
12: R = 5-methoxy-pyrazine-2-yl
13: R = 5-(2,2,2-trifluoroethoxy)pyrazine-2-yl
14: R = 5-fluoromethoxy-pyrazine-2-yl

[a]Reagents and conditions: (a) RCO_2H, EDC·HCl, aq HCl, THF or MeOH, 0 °C or 0 °C to rt, 49–100%.

The synthesis of the methoxy thiazine **15** started with (*R*)-*tert*-butylsulfinylketimine **25**,[27b,33] readily available from the corresponding ketone (Scheme 2). The lithium enolate of methyl 2-methoxyacetate was transformed to the corresponding titanium enolate using ClTi(O*i*-Pr)$_3$, which was reacted with the sulfinyl ketimine **25** to give the ester **26**.[27c] The ester group in **26** was reduced to the corresponding alcohol with $LiBH_4$ followed by cleavage of the sulfineamide group and subsequent thiourea formation using benzoyl isothiocyanate (BzNCS) to yield the thiourea **27**. Thiazine cyclization was accomplished with Ghosez's reagent[34] to give the thiazine **28**. Following deprotection of the benzoyl group in **28** with hydrazine monohydrate, thiazine **29** was nitrated with fuming nitric acid, and subsequent reduction of the nitro group and amide formation provided the desired thiazine **15**.

Scheme 2. Synthesis of Thiazine 15[a]

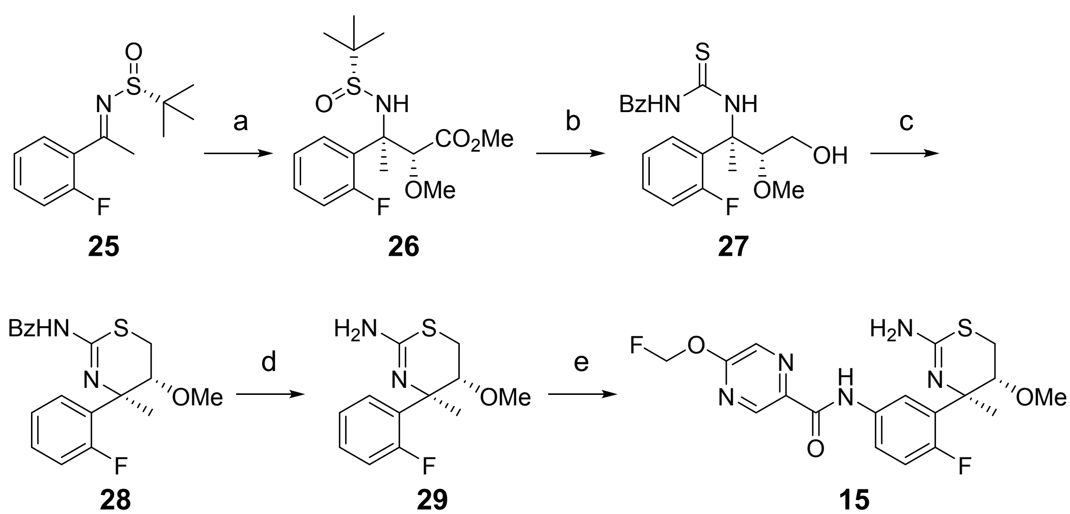

[a]Reagents and conditions: (a) *n*-BuLi, diisopropylamine, methyl 2-methoxyacetate, ClTi(O*i*-Pr)$_3$, THF, –78 °C, 72%; (b) (i) $LiBH_4$, MeOH, THF, 0 °C, (ii) 4 M HCl in 1,4-dioxane, MeOH, rt, (iii) BzNCS, DCM, rt, 82% over 3 steps; (c) Ghosez's reagent, DCM, rt, 90%; (d) hydrazine monohydrate, MeOH, THF, rt, 93%; (e) (i) HNO_3, H_2SO_4, TFA, –20 °C, (ii) Fe, NH_4Cl, EtOH, toluene, H_2O, 80 °C, (iii) 5-(fluoromethoxy)pyrazine-2-carboxylic acid, EDC·HCl, aq HCl, MeOH, 0 °C to rt, 58% over 3 steps.

As shown in Scheme 3, synthesis of thiazines **16** and **17** was achieved through a modified route to Scheme 2. Reaction of (*R*)-*tert*-butylsulfinylketimine **30**[35] and the titanium enolate of ethyl 2-phenylacetate yielded ester **31** as an inseparable 2:1 diastereomeric mixture. The *tert*-butylsulfinamide group in **31** was removed with HCl, and protection of the amine with Boc group provided **32** and **33**, which were separable by silicagel column chromatography. The ester groups in **32** and **33** were reduced to the corresponding alcohols, followed by deprotection of the Boc groups and thiourea formation to afford **34** and **35**, respectively. Thiazine formation using Ghosez's reagent[34] provided **36** and **37**, of which the benzoyl groups were deprotected, followed by introduction of an azide group with sodium azide and subsequent reduction of the azide group to provide the corresponding anilines. Finally, amide coupling of the anilines afforded the target compounds **16** and **17**. The absolute and relative configurations were assigned based on the crystal structures of **16** and **17** bound to BACE1.

Scheme 3. Synthesis of Thiazines 16 and 17[a]

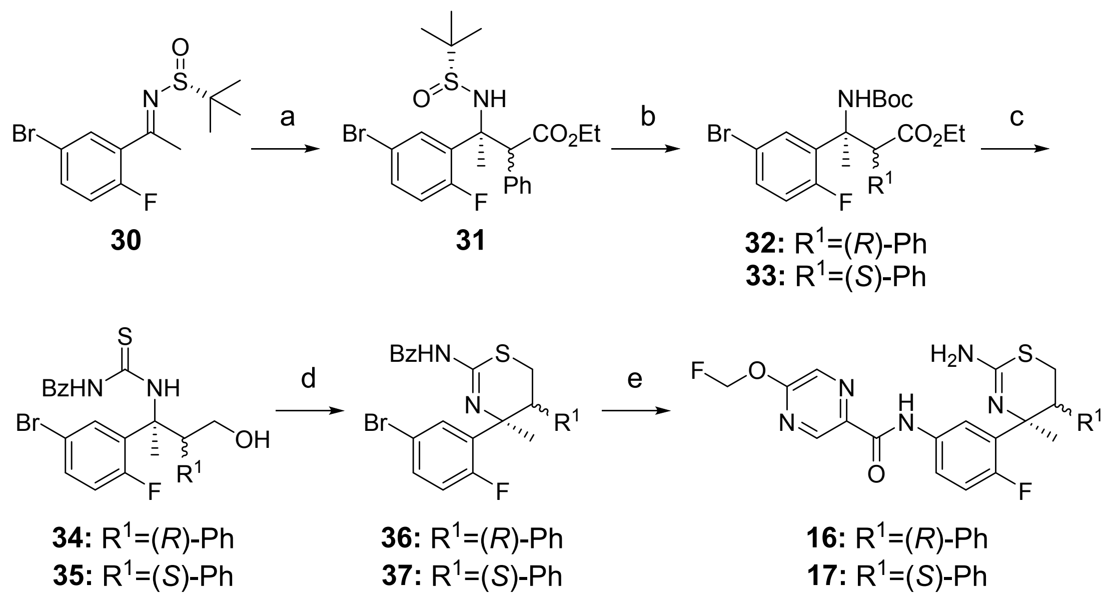

[a]Reagents and conditions: (a) *n*-BuLi, diisopropylamine, ethyl 2-phenylacetate, ClTi(O*i*-Pr)$_3$, THF, −78 °C, 91%, dr = 2:1; (b) (i) 4 M HCl in 1,4-dioxane, MeOH, rt, (ii) Boc$_2$O, MeOH, 60 °C, 57% and 28% (over 2 steps); (c) (i) LiBH$_4$, MeOH, THF, 0 °C, (ii) TFA, DCM, rt, (iii) BzNCS, DCM, rt, 78 and 87% over 3 steps; (d) Ghosez's reagent, 0 °C to rt, 90% and 81%; (e) (i) DBU, MeOH, 60 °C, (ii) NaN$_3$, CuI, (1*R*,2*R*)-*N*[1],*N*[2]-dimethylcyclohexane-1,2-diamine, sodium L-ascorbate, EtOH, H$_2$O, 100 °C, (iii) Fe, NH$_4$Cl, EtOH, H$_2$O , THF, 60 °C or Fe, NH$_4$Cl, EtOH, H$_2$O, THF, 60 °C, (iv) 5-(fluoromethoxy)pyrazine-2-carboxylic acid, EDC·HCl, aq HCl, MeOH, 0 °C, 46% and 55% over 4 steps.

As shown in Scheme 4, tetrahydro-2*H*-pyran substituted thiazine **18** was synthesized from the ketimine **25**. Reaction of **25** with ethyl 2-(tetrahydro-*2H*-pyran-4-yl)acetate yielded the ester **38** as an inseparable diasteromeric mixture. Cleavage of the sulfineamide group and subsequent Boc protection provided **39**. The ester group in **39** was reduced to the corresponding alcohol, of which the hydroxyl intramolecularly reacted with the Boc group to give carbamate **40**. The carbamate **40** was protected with a Boc group to give **41**. Ring opening of the carbamate **41** with K_2CO_2 in MeOH, deprotection of the Boc group, and subsequent thioureation provided **42**. Thiazine formation of the thiourea **42** was accomplished with *N*,*N*-diethylaminosulfur trifluoride (DAST) to give **43**.[27d] Boc protection of **43** allowed isolation of **44** and **45** as single isomers by silicagel column chromatography. Removal of the benzoyl group was conducted by hydrolysis using K_2CO_3 in MeOH following protection of the aminde NH with a Boc group. The resulting Boc group was deprotected with TFA to afford **46**, which was converted into the target compound **18** according to the established procedure as described in Schemes 1 and 3. The stereochemistry of **18** was confirmed by NOESY correlations using the intermediates **44** and **45** (Figures S1 and S2, see Supporting Information).

Scheme 4. Synthesis of Thiazines 18[a]

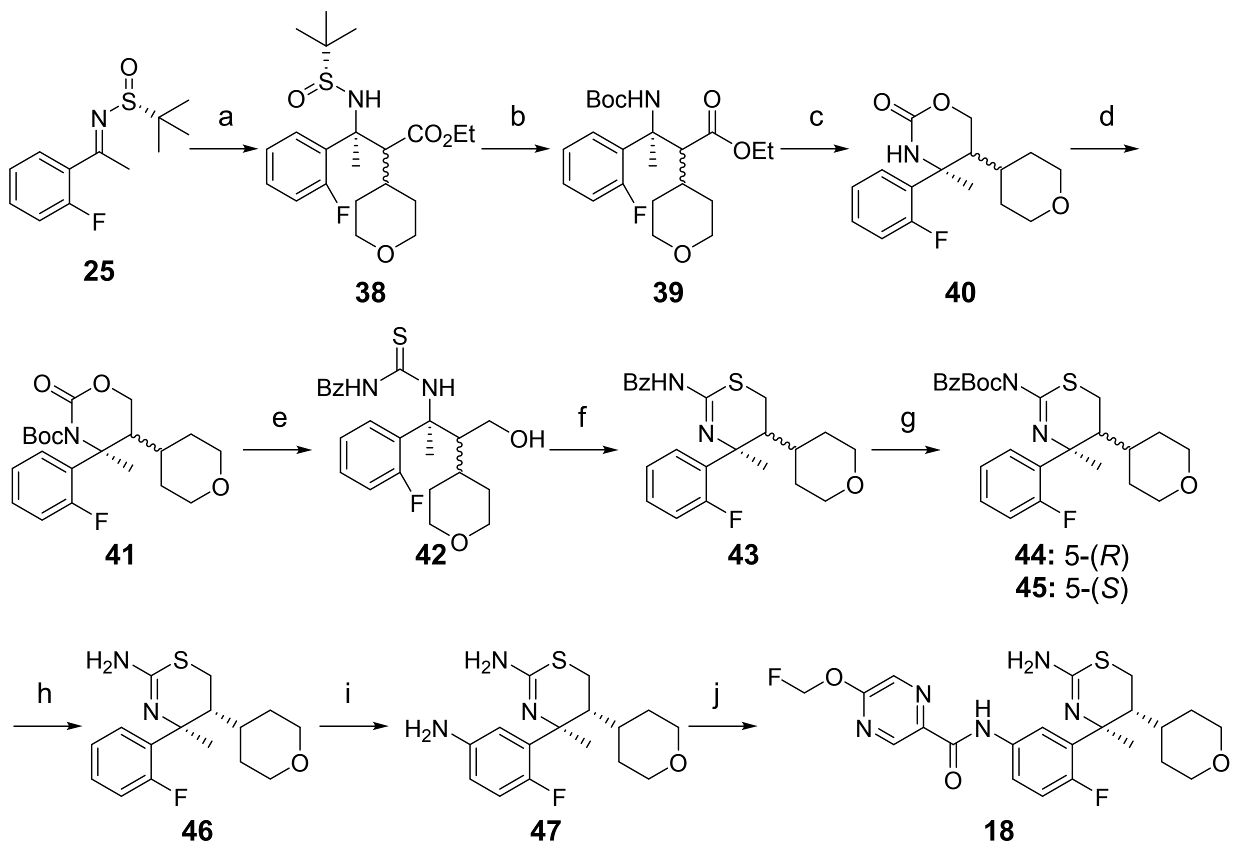

[a]Reagents and conditions: (a) *n*-BuLi, diisopropylamine, ethyl 2-(tetrahydro-*2H*-pyran-4-yl)acetate, $ClTi(O\textit{i}\text{-}Pr)_3$, THF, –78 °C, 43%, dr = 2.9:1; (b) (i) 4 M HCl in 1,4-dioxane, MeOH, rt, (ii) Boc_2O, THF, 60°C , 88% over 2 steps; (c) $LiBH_4$, MeOH, THF, 50 °C, 24%; (d) Boc_2O, DCM, THF, 60 °C, 73%; (e) (i) K_2CO_3, MeOH, rt, (ii) TFA, DCM, rt, (iii) BzNCS, DCM, rt, 49% over 3 steps; (f) DAST, DCM, 0 °C, 73%; (g) Boc_2O, THF, rt, 47% and 26%; (h) (i) K_2CO_3, MeOH, rt, (ii) TFA, DCM, rt, 91% over 2 steps; (i) (i) HNO_3, H_2SO_4, TFA, –20 °C, (ii) Fe, NH_4Cl, toluene, H_2O, 80 °C, 74% over 2 steps; (j) 5-(fluoromethoxy)pyrazine-2-carboxylic acid, EDC·HCl, aq HCl, MeOH, rt, 76%.

The synthesis of thiazine **19** started with sulfinyl ketimine **25** (Scheme 5). Addition of the titanium enolate of ethyl tetrahydro-2*H*-pyran-4-carboxylate to the ketimine **25**, cleavage of the sulfinaminde, and subsequent Boc protection afforded **49**. The subsequent steps to the target **19** were conducted according to the procedures described in Scheme 4. Similar to the syntheses of compounds **18** and **19**, the spiro thiazines **20** and **21** were synthesized according to Schemes 4 and 5 as shown in Schemes 6 and 7, respectively.

Scheme 5. Synthesis of Thiazines 19[a]

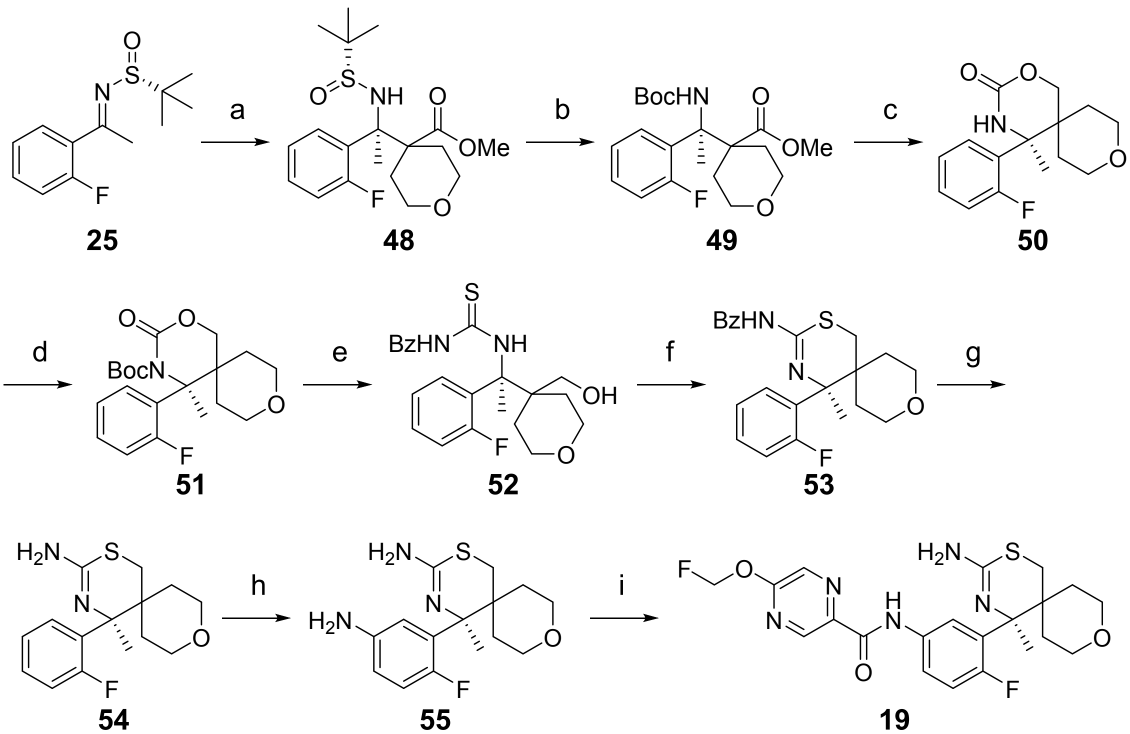

[a]Reagents and conditions: (a) *n*-BuLi, diisopropylamine, ethyl tetrahydro-*2H*-pyran-4-carboxylate, $ClTi(O\textit{i}\text{-}Pr)_3$, THF, –78 °C, 75%; (b) (i) 4 M HCl in 1,4-dioxane, MeOH, rt, (ii) Boc_2O, MeOH, 60 °C, quant. over 2 steps; (c) $LiBH_4$, MeOH, THF, 50 °C, 70%; (d) Boc_2O, DMAP, THF, 50 °C, 84%; (e) (i) K_2CO_3, MeOH, rt, (ii) TFA, DCM, rt, (iii) BzNCS, DCM, 0 °C to rt, 74% over 3 steps; (f) DAST, DCM, 0, 57%; (g) hydrazine monohydrate, MeOH, THF, rt , 71%; (h) (i) HNO_3, H_2SO_4, TFA, –20 °C to 0°C, (ii) Fe, NH_4Cl, toluene, H_2O, 80 °C, 78% over 2 steps; (i) 5-(fluoromethoxy)pyrazine-2-carboxylic acid, EDC·HCl, aq HCl, MeOH, 0 °C to rt, 81%.

Scheme 6. Synthesis of Thiazine 20[a]

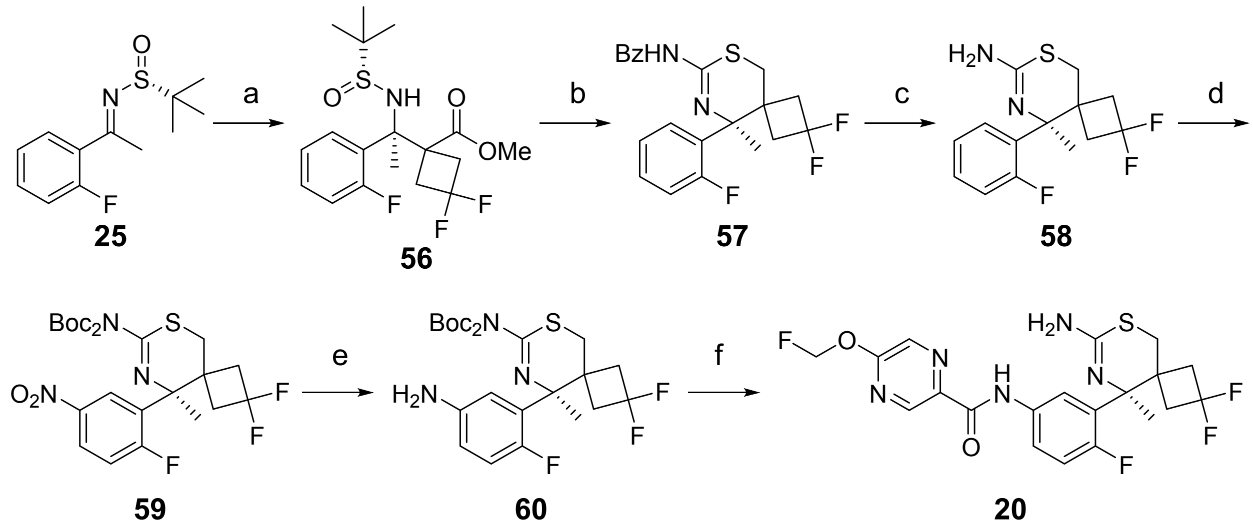

[a]Reagents and conditions: (a) *n*-BuLi, diisopropylamine, methyl 3,3-difluorocyclobutane-1-carboxylate, ClTi(O*i*-Pr)$_3$, THF, –78 °C, 39%; (b) (i) $LiBH_4$, MeOH, THF, 0 °C, (ii) 4 M HCl in 1,4-dioxane, MeOH, rt, (iii) BzNCS, DCM, rt, (iv) Ghosez's reagent, DCM, rt, 68% over 4 steps; (c) hydrazine monohydrate, MeOH, THF, rt, 96%; (d) (i) HNO_3, H_2SO_4, TFA, –20 °C to rt, (ii) Boc_2O, DMAP, THF, rt, 97% over 2 steps; (e) Fe, NH_4Cl, EtOH, toluene, H_2O, 60 °C, 79%; (f) (i) 5-(fluoromethoxy)pyrazine-2-carboxylic acid, HATU, *N*,*N*-diisopropylethylamine, MeOH, rt, 83%, (ii) TFA, DCM, rt, 93%.

Scheme 7. Synthesis of Thiazine 21[a]

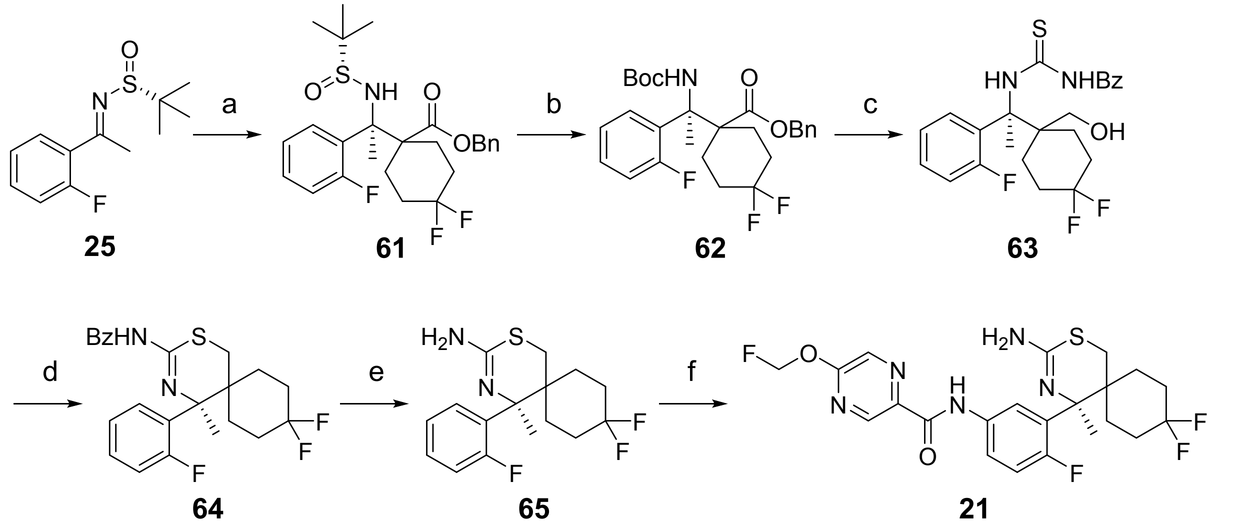

[a]Reagents and conditions: (a) *n*-BuLi, diisopropylamine, benzyl 4,4-difluorocyclohexane-1-carboxylate, ClTi(O*i*-Pr)$_3$, THF, –78 °C, 21%; (b) (i) 4 M HCl in 1,4-dioxane, MeOH, rt, (ii) Boc$_2$O, MeOH, 60 °C, 88% over 2 steps; (c) (i) LiBH$_4$, MeOH, THF, 0 °C to 40 °C, (ii) 4 M HCl in 1,4-dioxane, rt, (iii) BzNCS, DCM, 0 °C to rt, 54% over 3 steps; (d) DAST, DCM, 0 °C, 61%; (e) hydrazine hydrate, MeOH/THF, 50 °C, 73%; (f) (i) HNO$_3$, H$_2$SO$_4$, TFA, –15 °C, (ii) Fe, NH$_4$Cl, EtOH, toluene, H$_2$O, 80 °C, (iii) 5-(fluoromethoxy)pyrazine-2-carboxylic acid, EDC·HCl, aq HCl, MeOH, 0 °C to rt, 55% over 3 steps.

Scheme 8 describes the synthesis of the spiro thiazine **22** starting from the ketimine **25**. Like the other thiazines described above, the titanium enolate prepared from ethyl tetrahydro-2*H*-thiopyran-4-carboxylate reacted with **25** to afford ester **66**. Conversion of the ester **66** to the thiazine **70** was conducted via a similar reaction sequence as described in Schemes 4–7.The thiazine **70** was oxidized with *m*-CPBA to give **71**. Sulfone **71** was nitrated with fuming nitric acid followed by reduction of the nitro group and amide formation to provide the desired spiro thiazine **22**.

Scheme 8. Synthesis of spiro-Thiazine 22[a]

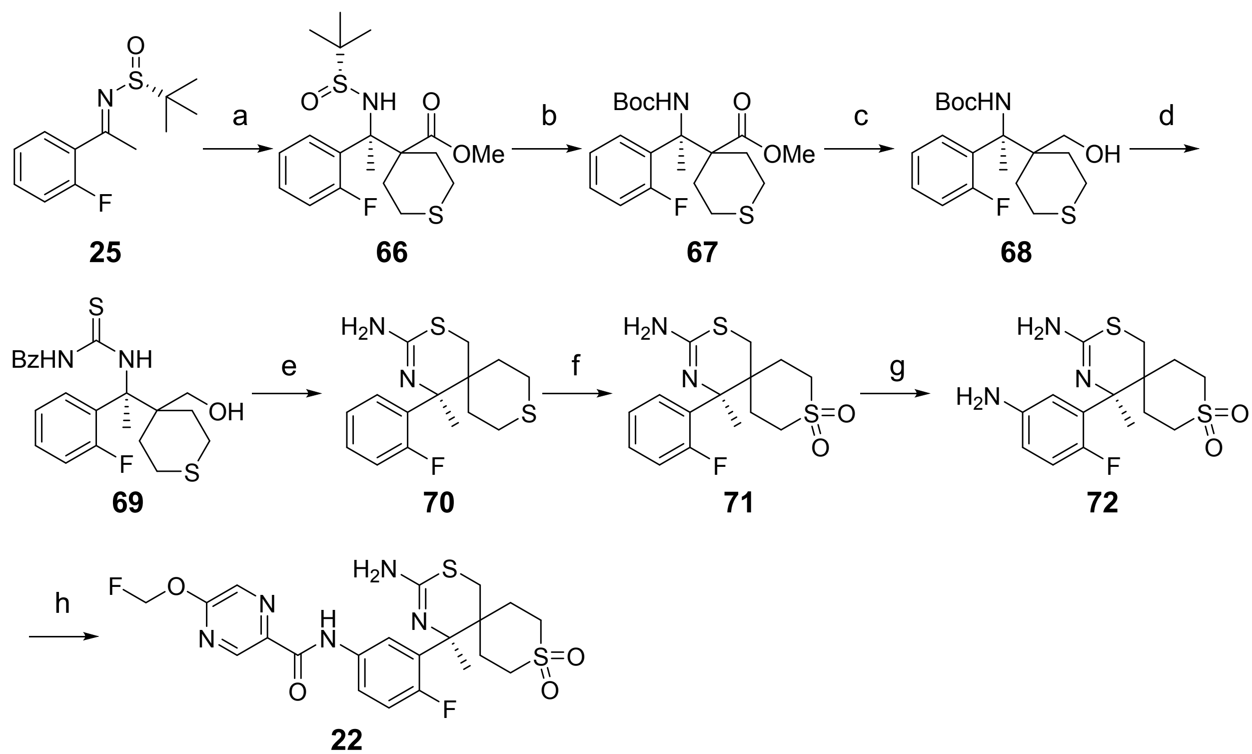

[a]Reagents and conditions: (a) *n*-BuLi, diisopropylamine, methyl tetrahydro-2*H*-thiopyran-4-carboxylate, ClTi(O*i*-Pr)$_3$, THF, –78 °C, 59%; (b) (i) 4 M HCl in 1,4-dioxane, MeOH, rt, (ii) Boc$_2$O, MeOH, 50 °C, 94% over 2 steps; (c) LiBH$_4$, MeOH/THF, 0 °C to 50 °C, 48%; (d) (i) TFA, DCM, rt, (ii) BzNCS, DCM, rt, 70% over 2 steps; (e) (i) DAST, DCM, rt, (ii) hydrazine monohydrate, MeOH, THF, 40 °C, 16% over 2 steps; (f) *m*-CPBA, DMC, 0 °C, 90%; (g) (i) HNO$_3$, H$_2$SO$_4$, TFA, –10 °C to 0°C, (ii) Fe, NH$_4$Cl, toluene, H$_2$O, 80 °C, 77% over 2 steps; (h) 5-(fluoromethoxy)pyrazine-2-carboxylic acid, EDC·HCl, aq HCl, MeOH, 0 °C to rt, 66%.

CONCLUSIONS

Utilizing structure-based drug design, a unique thiazine-based selective BACE1 inhibitor was discovered starting with **8**. It possessed a biochemical BACE1/2 selectivity of 1.6-fold, leading to the discovery of the spirocycle-based inhibitors **21** and **22** with more than 100- and 500-fold selectivity over BACE2 in the biochemical and the binding assays, respectively. This improved selectivity was rationalized by interaction of the spirocycle with the flap, where BACE1 was likely to accommodate larger substituents than BACE2 due to the difference in conformational flexibility. The cocrystal structures of **22** bound to both the enzymes confirmed a higher energetic penalty, as indicated by the B-factors, around the flap in the **22**-bound BACE2 structure than that in BACE1, resulting in loss of BACE2 potency and thereby increased selectivity. The structural insights, the high-resolution inhibitor-bound structures, as well as the selective BACE1 inhibitors, such as **21** and **22**, should aid structure-based discovery of novel selective BACE1 inhibitors, which eventually could lead to a next generation of safer BACE1 inhibitors.

EXPERIMENTAL SECTION

General Chemistry. All commercial chemicals were used as received. Column chromatography was carried out on an automated purification system using Fuji Silysia or Yamazen prepacked silica gel columns. ^{1}H NMR and ^{13}C NMR spectra were recorded on a Bruker Advance 400 and 100 MHz, respectively. Spectral data are reported as follows: chemical shift (as ppm referenced to tetramethylsilane), integration value, multiplicity (s = singlet, d = doublet, dd = double doublet, ddd = double double doublet, dt = double triplet, t = triplet, q = quartet, m = multiplet, br = broad peak), and coupling constant. Analytical LC/MS was performed on a Shimadzu UFLC system coupled with a LCMS-2020 mass spectrometer, SPD-M20A photodiode array detector (detection at 254 nm), LC-20AD binary gradient module, and SIL-20AC sample manager, which was operated on a Shimadzu Shim-pack XR-ODS column (C_{18}, 2.2 μm, 3.0 × 50 mm) with a linear gradient from 10% to 100% B over 3 min and then 100% B for 1 min (A = H_2O + 0.1% formic acid, B = MeCN + 0.1% formic acid) at a flow rate of 1.6 mL/min. Purities of all final compounds were determined to be greater than 95%. High resolution mass spectra were recorded on a Thermo Fisher Scientific LTQ Orbitrap with electrospray ionization.

General Procedure for Condensation with Carboxylic Acids. To a solution of aniline (1.0 eq), carboxylic acid (1.0–1.05 eq), and HCl (2 M in water, 1.0 eq) in MeOH was added EDC·HCl (1.1 eq) at 0 °C (or room temperature). The mixture was stirred at room temperature for 1 h and treated with aqueous $NaHCO_3$ solution. The aqueous layer was separated and extracted with EtOAc. The combined organic layers were washed with water and brine, dried over Na_2SO_4, filtered, and evaporated. The residue was purified by flash column chromatography and/or crystallization to obtain the target compound.

(*S*)-*N*-(3-(2-Amino-4-methyl-5,6-dihydro-*4H*-1,3-thiazin-4-yl)-4-fluorophenyl)-5-chloropicolinamide (8). Compound **8** was prepared from **23** (150 mg, 0.627 mmol) according to the general procedure (220 mg, 92%). White solid. ^{1}H NMR (400 MHz, $CDCl_3$) δ 9.80 (1H, s), 8.56 (1H, d, *J* = 2.4 Hz), 8.24 (1H, d, *J* = 8.4 Hz), 8.00 (1H, ddd, *J* = 8.8, 4.0, 2.8 Hz), 7.87 (1H, dd, *J* = 8.4, 2.4 Hz), 7.41 (1H, dd, *J* = 7.0, 2.8 Hz), 7.06 (1H, dd, *J* = 11.7, 8.8 Hz), 4.46 (2H, br s), 2.98 (1H, ddd, *J* = 12.2, 6.7, 3.6 Hz), 2.74 (1H, ddd, *J* = 12.2, 10.4, 3.6 Hz), 2.43 (1H, ddd, *J* = 14.0, 6.7, 3.6 Hz), 1.94 (1H, ddd, *J* = 14.0, 10.4, 3.6 Hz), 1.63 (3H, d, *J* = 1.0). MS-ESI (*m/z*): 379 $[M + H]^+$.

(*S*)-*N*-(3-(2-Amino-4-methyl-5,6-dihydro-*4H*-1,3-thiazin-4-yl)-4-fluorophenyl)-5-fluoropicolinamide (9). Compound **9** was prepared from **23** (50.0 mg, 0.209 mmol) according to the general procedure (37.2 mg, 49%). White solid. ^{1}H NMR (400 MHz, $CDCl_3$) δ 9.78 (1H, s), 8.46 (1H, d, *J* = 2.6 Hz), 8.33 (1H, dd, *J* = 8.6, 4.6 Hz), 8.01–7.97 (1H, m), 7.59 (1H, td, *J* = 8.4, 2.6 Hz), 7.40 (1H, dd, *J* = 6.9, 2.8 Hz), 7.06 (1H, dd, *J* = 11.6, 8.7 Hz), 2.98 (1H, ddd, *J* = 11.5, 6.7, 3.9 Hz), 2.78–2.71 (1H, m), 2.49–2.43 (1H, m), 1.94 (1H, ddd, *J* = 14.2, 10.8, 3.8 Hz), 1.64 (3H, s).MS-ESI (*m/z*): 363 $[M + H]^+$.

(*S*)-*N*-(3-(2-Amino-4-methyl-5,6-dihydro-*4H*-1,3-thiazin-4-yl)-4-fluorophenyl)-5-cyanopicolinamide (10). Compound **10** was prepared from **23** (130 mg, 0.543 mmol) according to the general procedure (202 mg, quant.). White solid. ^{1}H NMR (400 MHz, $CDCl_3$) δ 9.83 (1H, s), 8.89 (1H, d, *J* = 2.0 Hz), 8.43 (1H, d, *J* = 8.2 Hz), 8.20 (1H, dd, *J* = 8.2, 2.0 Hz), 7.99 (1H, ddd, *J* = 8.8, 4.0, 2.8 Hz), 7.45 (1H, dd, *J* = 7.0, 2.8 Hz), 7.08 (1H, dd, *J* = 11.5, 8.8 Hz), 4.47 (2H, br s), 2.99 (1H, ddd, *J* = 12.2, 6.8, 3.6 Hz), 2.74 (1H, ddd, *J* = 12.2, 10.4, 3.6 Hz), 2.42 (1H, ddd, *J* = 14.0, 6.8, 3.6 Hz), 1.95 (1H, ddd, *J* = 14.0, 10.4, 3.6 Hz), 1.63 (3H, d, *J* = 1.1). MS-ESI (*m/z*): 370 $[M + H]^+$.

(*S*)-*N*-(3-(2-Amino-4-methyl-5,6-dihydro-*4H*-1,3-thiazin-4-yl)-4-fluorophenyl)-5-(difluoromethyl)pyrazine-2-carboxamide (11). Compound **11** was prepared from **23** (51.0 mg, 0.213 mmol) according to the general procedure (63.8 mg, 78%). Pale yellow solid. ^{1}H NMR (400 MHz, $CDCl_3$) δ 9.64 (1H, br s), 9.53 (1H, s), 8.93 (1H, s), 8.00 (1H, ddd, *J* = 8.8, 3.9, 2.8 Hz), 7.44 (1H, dd, *J* = 6.8, 2.8 Hz), 7.09 (1H, dd, *J* = 11.5, 8.8 Hz), 6.79 (1H, t, *J* = 54.5 Hz), 3.00 (1H, ddd, *J* = 12.2, 6.7, 3.5 Hz), 2.75 (1H, ddd, *J* = 12.2, 10.4, 3.5 Hz), 2.44 (1H, ddd, *J* = 14.0, 6.7, 3.5 Hz), 1.96 (1H, ddd, *J* = 14.0, 10.4, 3.5 Hz), 1.66 (3H, s). MS-ESI (*m/z*): 396 $[M + H]^+$.

(*S*)-*N*-(3-(2-Amino-4-methyl-5,6-dihydro-*4H*-1,3-thiazin-4-yl)-4-fluorophenyl)-5-methoxypyrazine-2-carboxamide (12). Compound **12** was prepared from **23** (130 mg, 0.543 mmol) according to the general procedure (190 mg, 93%). White solid. ^1H NMR (400 MHz, $CDCl_3$) δ 9.48 (1H, s), 9.01 (1H, d, *J* = 1.3 Hz), 8.15 (1H, d, *J* = 1.3 Hz), 7.99 (1H, ddd, *J* = 8.9, 3.9, 2.8 Hz), 7.37 (1H, dd, *J* = 7.0, 2.8 Hz), 7.05 (1H, dd, *J* = 11.7, 8.9 Hz), 4.44 (2H, br s), 4.07 (3H, s), 2.98 (1H, ddd, *J* = 12.2, 6.6, 3.7 Hz), 2.74 (1H, ddd, *J* = 12.2, 10.4, 3.5 Hz), 2.43 (1H, ddd, *J* = 13.9, 6.6, 3.5 Hz), 1.93 (1H, ddd, *J* = 13.9, 10.4, 3.7 Hz), 1.62 (3H, d, *J* = 0.9 Hz). MS-ESI (*m/z*): 376 $[M + H]^+$.

(*S*)-*N*-(3-(2-Amino-4-methyl-5,6-dihydro-4*H*-1,3-thiazin-4-yl)-4-fluorophenyl)-5-(2,2,2-trifluoroethoxy)pyrazine-2-carboxamide (13). Compound **13** was prepared from **23** according to the general procedure (76.0 mg, 86%). White solid. ^1H NMR (400 MHz, $CDCl_3$) δ 9.47 (1H, s), 9.02 (1H, d, *J* = 1.3 Hz), 8.31 (1H, d, *J* = 1.3 Hz), 7.98 (1H, ddd, *J* = 8.7, 3.9, 2.9 Hz), 7.40 (1H, dd, *J* = 7.0, 2.8 Hz), 7.06 (1H, dd, *J* = 11.6, 8.7 Hz), 4.86 (2H, q, *J* = 8.2 Hz), 2.99 (1H, ddd, *J* = 12.2, 6.6, 3.7 Hz), 2.75 (1H, ddd, *J* = 12.2, 10.5, 3.5 Hz), 2.43 (1H, ddd, *J* = 14.0, 6.6, 3.4 Hz), 1.95 (1H, ddd, *J* = 14.0, 10.5, 3.7 Hz), 1.63 (3H, d, *J* = 1.0 Hz). MS-ESI (*m/z*): 444 $[M + H]^+$.

(*S*)-*N*-(3-(2-Amino-4-methyl-5,6-dihydro-*4H*-1,3-thiazin-4-yl)-4-fluorophenyl)-5-(fluoromethoxy)pyrazine-2-carboxamide (14). Compound **14** was prepared from **23** (150 mg, 0.627 mmol) according to the general procedure (219 mg, 89%). White solid. ^1H NMR (400 MHz, $CDCl_3$) δ 9.47 (1H, s), 9.08 (1H, d, *J* = 1.2 Hz), 8.28 (1H, d, *J* = 1.2 Hz), 7.99 (1H, ddd, *J* = 8.7, 3.9, 2.9 Hz), 7.39 (1H, dd, *J* = 7.0, 2.9 Hz), 7.06 (1H, dd, *J* = 11.7, 8.7 Hz), 6.22–6.08 (2H, m), 4.46 (2H, s), 2.98 (1H, ddd, *J* = 12.2, 6.7, 3.7 Hz), 2.74 (1H, ddd, *J* = 12.2, 10.5, 3.5 Hz), 2.42 (1H, ddd, J = 13.9, 6.7, 3.5 Hz), 1.94 (1H, ddd, J = 13.9, 10.5, 3.7 Hz), 1.63 (3H, d, J = 0.9 Hz). MS-ESI (m/z): 394 $[M + H]^+$.

_N_-(3-((4_S_,5_R_)-2-Amino-4-methyl-5-phenyl-5,6-dihydro-4_H_-1,3-thiazin-4-yl)-4-fluorophenyl)-5-(fluoromethoxy)pyrazine-2-carboxamide (16). A mixture of **36** (267 mg, 0.553 mmol) and DBU (83.0 μL, 0.553 mmol) in MeOH (8.0 mL) was stirred at 60 °C for 6 h. The mixture was cooled to room temperature and treated with HCl solution (2 M in water). The mixture was diluted with Et_2O, and the organic layers were back extracted with H_2O. The aqueous layer was basified with K_2CO_3 and extracted with EtOAc. The organic layers were washed with water and concentrated to give the crude compound (201 mg) as a colorless oil. A mixture of this crude compound (108 mg), CuI (10.8 mg, 0.057 mmol), (1_R_,2_R_)-N^1,N^2-dimethylcyclohexane-1,2-diamine (13.5μL, 0.085 mmol), NaN_3 (74.0 mg, 1.14 mmol), and sodium L-ascorbate (5.64 mg, 0.0280 mmol) in EtOH and H_2O (1.5 mL/0.5 mL) was stirred at 100 °C for 1.5 h. The reaction mixture was quenched with water, and the aqueous layer was extracted with EtOAc. The organic layers were washed with water and evaporated to give the crude compound (77.4 mg) as an orange amorphous substance. A suspension of this crude compound, Fe (101 mg, 1.84 mmol), and NH_4Cl (146 mg, 2.72 mmol) in EtOH/THF/H_2O (1.0 mL/0.5 mL/0.5 mL) was stirred at 60 °C for 1.5 h. The mixture was cooled to room temperature, diluted with aqueous K_2CO_3 solution, and filtered through Celite. The aqueous layer was extracted with EtOAc. The organic layers were washed with water and concentrated to give the crude compound (63.4 mg) as a white amorphous substance. This crude compound was subjected to the amide coupling reaction conditions according to the general procedure outlined above to give **16** (35.9 mg, 46% over 4 steps) as a tan solid. [1]H NMR (400 MHz, $CDCl_3$) δ 9.43 (1H, br s), 9.08 (1H, d, *J* = 1.3 Hz), 8.29 (1H, d, *J* = 1.3 Hz), 7.92–7.88 (1H, m), 7.32 (1H, dd, *J* = 6.9, 2.6 Hz), 7.25–7.22 (3H, m), 7.18–7.16 (2H, m), 7.02 (1H, dd, *J* = 11.7, 8.7 Hz), 6.15 (2H, d, *J* = 51.1 Hz), 3.64 (1H, dd, *J* = 7.1, 4.5 Hz), 3.30 (1H, dd, *J* = 12.3, 7.1 Hz), 3.11 (1H, dd, *J* = 12.3, 4.5 Hz), 1.56 (3H, d, *J* = 1.6 Hz). MS-ESI (*m/z*): 470 $[M + H]^+$.

***N*-(3-((4*S*,5*S*)-2-Amino-4-methyl-5-phenyl-5,6-dihydro-4*H*-1,3-thiazin-4-yl)-4-fluorophenyl)-5-(fluoromethoxy)pyrazine-2-carboxamide (17).** A mixture of **37** (179 mg, 0.371 mmol) and DBU (55.9 μL, 0.371 mmol) in MeOH (5.4 mL) was stirred at 60 °C for 11 h. The mixture was cooled to room temperature and treated with HCl solution (2 M in water). The mixture was diluted with Et_2O, and the organic layers were back extracted with H_2O. The aqueous layer was basified with K_2CO_3, and the aqueous layer was extracted with EtOAc. The organic layers were washed with water and concentrated to give the crude compound (137 mg) as a white amorphous substance. A mixture of this crude compound, CuI (13.8 mg, 0.072 mmol), (1*R*,2*R*)-N^1,N^2-dimethylcyclohexane-1,2-diamine (17.1 μL, 0.108 mmol), NaN_3 (94.0 mg, 1.45 mmol) and sodium L-ascorbate (7.16 mg, 0.0360 mmol) in EtOH/H_2O (1.9 mL/0.7 mL) was stirred at 100 °C for 2 h. The reaction mixture was quenched with water, and the aqueous layer was extracted with EtOAc. The organic layers were washed with water and evaporated to give the crude compound (109 mg) as a tan amorphous substance. A suspension of this crude compound, Fe (143 mg, 2.56 mmol), and NH_4Cl (205 mg, 3.84 mmol) in EtOH/H_2O (1.5 mL/0.8 mL) was stirred at 60 °C for 5 h. The mixture was cooled to room temperature and diluted with aqueous K_2CO_3 solution and filtered through Celite. The aqueous layer was extracted with EtOAc. The organic layers were washed with water and concentrated to give the crude compound (95.5 mg) as a tan solid. This crude compound was subjected to the amide coupling reaction conditions according to the general procedure outlined above to give **17** (52.8 mg, 55% over 4 steps) as a tan solid. ^{1}H NMR (400 MHz, $CDCl_3$) δ 9.37 (1H, br s), 9.05 (1H, s), 8.27 (1H, s), 7.91–7.88 (1H, m), 7.59–7.56 (1H, m), 7.06–7.04 (5H, m), 6.92–6.87 (1H, m), 6.14 (3H, d, *J* = 51.2 Hz), 4.50 (2H, br s), 3.78–3.72 (2H, m), 3.14–3.11 (1H, m), 1.71 (3H, s). MS-ESI (*m/z*): 470 [M + H]$^+$.

(*R*)-*N*-(3-(3-Amino-5-methyl-9,9-dioxido-2,9-dithia-4-azaspiro[5.5]undec-3-en-5-yl)-4-fluorophenyl)-5-(fluoromethoxy)pyrazine-2-carboxamide (22). Compound **22** was prepared from **72** (48.6 mg, 0.136 mmol) according to the general procedure (45.8 mg, 66%). Pale yellow solid. ^{1}H NMR (400 MHz, $CDCl_3$) δ 9.48 (1H, s), 9.09 (1H, d, *J* = 1.3 Hz), 8.30 (1H, d, *J* = 1.3 Hz), 7.77–7.71 (2H, m), 7.06 (1H, dd, *J* = 12.2, 8.8 Hz), 6.15 (2H, d, *J* = 51.1 Hz), 3.16 (1H, d, *J* = 13.4 Hz), 3.07–2.89 (5H, m), 2.38–2.30 (1H, m), 2.24–2.15 (2H, m), 1.94–1.90 (1H, m), 1.73 (3H, d, *J* = 4.5 Hz). ^{13}C NMR (100 MHz, $CDCl_3$) δ 160.4, 159.4 (d, *J* = 2.9 Hz), 157.1 (d, *J* = 245.8 Hz), 148.4, 141.8, 139.7, 133.2, 133.2 (d, *J* = 2.9 Hz), 130.9 (d, *J* = 12.5 Hz), 123.7, 121.1 (d, *J* = 8.8 Hz), 117.3 (d, *J* = 27.8 Hz), 95.8 (d, *J* = 223.7 Hz), 63.1, 47.3, 47.2, 33.3, 29.1 (d, *J* =3.7 Hz), 27.2, 26.9, 24.0. HRMS-ESI (*m/z*): [M + H]$^+$ calcd for $C_{21}H_{24}O_4N_5F_2S_2^+$ 512.1232, found 512.1231.

Ethyl (3*S*)-3-(5-bromo-2-fluorophenyl)-3-(((*R*)-*tert*-butylsulfinyl)amino)-2-phenylbutanoate (31). To a solution of diisopropylamine (2.40 mL, 17.1 mmol) in THF (16 mL) was added dropwise *n*-BuLi (1.54 M in hexane; 10.5 mL, 16.2 mmol) at –78 °C. The mixture was allowed to warm to 0 °C and stirred at the same temperature for 20 min. The mixture was again cooled to –78 °C, and a solution of ethyl 2-phenylacetate (2.00 g, 12.2 mmo) in THF (7.8 mL) was added dropwise to the mixture. After being stirred at the same temperature for 40 min, a solution of $ClTi(Oi\text{-}Pr)_3$ (4.08 mL, 17.1 mmol) in THF (7.8 mL) was added dropwise at –78 °C. The mixture was stirred at the same temperature for 10 min, and then **30** (1.30 g, 4.06 mmol) in THF (7.8 mL) was added dropwise. After being stirred for 15 min, the mixture was quenched with aqueous NH_4Cl solution. The resulting mixture was filtered through Celite and evaporated. The residue was purified by flash column chromatography (silica gel; EtOAc/hexane, gradient: 10–40% EtOAc) to give **31** (1.78 g, 91%) as a yellow oil. 1.7:1 diastereomeric mixture. ^1H NMR (400 MHz, $CDCl_3$) δ 7.41–7.34 (2H, m), 7.31–7.20 (4H, m), 7.09–7.06 (1H, m), 6.97–6.90 (1H, m), 5.29 (1H, s), 4.46 (1H, d, J = 1.1 Hz), 4.18–4.02 (2H, m), 1.87 (3H, s), 1.27 (9H, s), 1.13 (3H, t, J = 7.1 Hz).

Ethyl (2*R*,3*S*)-3-(5-bromo-2-fluorophenyl)-3-((*tert*-butoxycarbonyl)amino)-2-phenylbutanoate (32) and ethyl (2*S*,3*S*)-3-(5-bromo-2-fluorophenyl)-3-((*tert*-butoxycarbonyl)amino)-2-phenylbutanoate (33). A mixture of **31** (900 mg, 1.86 mmol) and HCl (4 M in 1,4-dioxane; 697 µL, 2.79 mmol) in MeOH (18 mL) was stirred at room temperature for 1 h. The mixture was diluted with Et_2O, and then the organic layers were back extracted with H_2O. The aqueous layer was basified with K_2CO_3, which was extracted with EtOAc. The organic layers were washed with water and concentrated to give the crude compound (689 mg) as a colorless oil with a diastereomeric ratio of 2:1. A mixture of this crude compound and Boc_2O (2.11 mL, 9.08 mmol) was stirred at 60 °C for 6 h. The mixture was cooled to room temperature, and then 1-methylpiperazine (805 μL, 7.26 mmol) was added to this mixture. The resulting mixture was evaporated, and the residue was purified by flash column chromatography (silica gel; 10% EtOAc in hexane) to give **32** (507 mg, 57% over 2 steps) as a white amorphous substance and **33** (252 mg, 28 over 2 steps) as a white amorphous substance. ^{1}H NMR (400 MHz, $CDCl_3$; major isomer) δ 7.49–7.46 (2H, m), 7.38–7.34 (5H, m), 6.95 (1H, dd, J = 11.3, 8.4 Hz), 6.86 (1H, br s), 4.15 (1H, s), 4.03–3.95 (1H, m), 3.86–3.78 (1H, m), 1.75 (3H, d, J = 2.1 Hz), 1.45 (9H, br s), 0.92 (3H, t, J = 7.1 Hz). ^{1}H NMR (400 MHz, $CDCl_3$; minor isomer) δ 7.26–7.20 (4H, m), 7.13–7.11 (2H, m), 7.02 (1H, br s), 6.87 (1H, dd, J = 12.0, 8.7 Hz), 6.12 (1H, br s), 4.22–4.15 (1H, m), 4.11 (1H, s), 4.07–4.01 (1H, m), 1.99 (3H, br s), 1.38 (9H, br s), 1.18 (3H, t, J = 6.8 Hz).

***N*-(((2*S*,3*R*)-2-(5-Bromo-2-fluorophenyl)-4-hydroxy-3-phenylbutan-2-yl)carbamothioyl)benzamide (34).** To a solution of **32** (455 mg, 0.948 mmol) and MeOH (163 μL, 2.85 mmol) in THF (2.3 mL) was added $LiBH_4$ (3.0 M in THF; 948 μL, 2.85 mmol) at 0 °C. After stirring for 19 h at room temperature, the mixture was cooled to 0 °C and then diluted with H_2O and AcOH. The aqueous layer was separated and extracted with EtOAc. The organic layers were washed with water and concentrated to give the crude compound (427 mg) as a white amorphous substance. To a solution of this crude and other batch prepared according to the above method (473 mg) in DCM (4.7 mL) was added TFA (832 μL, 10.8 mmol) at room temperature. After stirring for 1 h at the same temperature, the reaction mixture was quenched with aqueous K_2CO_3 solution. The aqueous layer was separated and extracted with DCM. The organic layers were dried over Na_2SO_4, filtered, and evaporated to give the crude compound (367 mg) as a white amorphous substance. To a solution of this crude compound in DCM (3.7 mL) was added BzNCS (174 μL, 1.30 mmol) at 0 °C. After stirring at room temperature for 1 h, the reaction mixture was concentrated. The residue was purified by flash column chromatography (silica gel; EtOAc/hexane, gradient: 10–45% EtOAc) to give **34** (414 mg, 78% over 3 steps) as a white amorphous substance. ^{1}H NMR (400 MHz, $CDCl_3$) δ 11.91 (1H, s), 8.80 (1H, s), 7.89–7.87 (2H, m), 7.66–7.61 (1H, m), 7.55–7.51 (2H, m), 7.29–7.24 (1H, m), 7.22–7.20 (3H, m), 7.08–7.05 (2H, m), 7.01–6.99 (1H, m), 6.85 (1H, dd, *J* = 11.9, 8.7 Hz), 4.36–4.29 (1H, m), 4.27–4.21 (1H, m), 3.60 (1H, t, *J* = 7.0 Hz), 2.17 (3H, s), 1.71–1.69 (1H, m).

***N*-(((2*S*,3*S*)-2-(5-Bromo-2-fluorophenyl)-4-hydroxy-3-phenylbutan-2-yl)carbamothioyl)benzamide (35).** To a solution of **33** (252 mg, 0.524 mmol) and MeOH (90.0 μL, 1.57 mmol) in THF (2.5 mL) was added $LiBH_4$ (3.0 M in THF; 524 μL, 1.57 mmol) at 0 °C. After stirring for 1 day at room temperature, the mixture was cooled to 0 °C and diluted with H_2O and AcOH. The aqueous layer was separated and extracted with EtOAc. The organic layers were washed with water and concentrated to give the crude compound (234 mg) as a white amorphous substance. To a solution of this crude compound in DCM (2.3 mL) was added TFA (404 μL, 5.25 mmol) at room temperature. After stirring for 2 h at the same temperature, the reaction mixture was quenched with aqueous K_2CO_3 solution. The aqueous layer was separated and extracted with DCM. The organic layers were dried over Na_2SO_4, filtered, and evaporated to give the crude compound (189 mg) as a white amorphous substance. To a solution of this crude compound in DCM (1.9 mL) was added BzNCS (84 μL, 0.628 mmol) at 0 °C. After stirring at room temperature for 1 h, the reaction mixture was concentrated. The residue was treated with IPE and collected on a glass filter to give the target compound as a pale yellow solid. The filtrate was purified by flash column chromatography (silica gel; EtOAc/hexane, gradient: 10–40% EtOAc) to afford the target compound as well. The solid collected and the purified compound were combined to give **35** (229 mg, 87% over 3 steps)as a yellow amorphous substance. ^{1}H NMR (400 MHz, $CDCl_3$) δ 11.43 (1H, s), 8.70 (1H, s), 7.82–7.80 (2H, m), 7.62–7.59 (1H, m), 7.52–7.48 (2H, m), 7.43–7.35 (6H, m), 7.31–7.29 (1H, m), 6.93 (1H, dd, *J* = 11.9, 8.7 Hz), 4.10–4.04 (1H, m), 3.87–3.81 (1H, m), 3.62 (1H, dd, *J* = 9.2, 4.6 Hz), 2.16 (3H, s).

***N*-((4*S*,5*R*)-4-(5-Bromo-2-fluorophenyl)-4-methyl-5-phenyl-5,6-dihydro-4*H*-1,3-thiazin-2-yl)benzamide (36).** To a solution of compound **34** (310 mg, 0.617 mmol) in DCM (3.1 mL) was added Ghosez's reagent (245 μL, 1.85 mmol) at 0 °C. After stirring for 1.5 h at room temperature, the reaction mixture was treated with aqueous $NaHCO_3$ solution. The aqueous layer was extracted with EtOAc. The organic layers were washed with water and evaporated. The residue was purified by flash column chromatography (silica gel; EtOAc/hexane, gradient: 10–30% EtOAc) to give **36** (267mg, 90%) as a colorless oil. ^{1}H NMR (400 MHz, $CDCl_3$) δ 8.24 (2H, d, *J* = 7.3 Hz), 7.54–7.50 (1H, m), 7.47–7.43 (3H, m), 7.35 (1H, dd, *J* = 7.1, 2.3 Hz), 7.31–7.25 (5H, m), 7.02 (1H, dd, *J* = 11.9, 8.8 Hz), 3.95–3.93 (1H, m), 3.26 (1H, dd, *J* = 13.1, 5.6 Hz), 3.15 (1H, dd, *J* = 13.1, 4.6 Hz), 1.61 (3H, s).

***N*-((4*S*,5*S*)-4-(5-Bromo-2-fluorophenyl)-4-methyl-5-phenyl-5,6-dihydro-4*H*-1,3-thiazin-2-yl)benzamide (37).** To a solution of compound **35** (229 mg, 0.458 mmol) in DCM (2.3 mL) was added Ghosez's reagent (182 μL, 1.37 mmol) at 0 °C. After stirring for 3 h at room temperature, the reaction mixture was treated with aqueous $NaHCO_3$ solution. The aqueous layer was extracted with EtOAc. The organic layers were washed with water and evaporated. The residue was purified by flash column chromatography (silica gel; EtOAc/hexane, gradient: 0–20% EtOAc) to give **37** (179 mg, 81%) as a white amorphous substance. ^{1}H NMR (400 MHz, $CDCl_3$) δ 8.17–8.15 (2H, m), 7.55–7.51 (1H, m), 7.48–7.44 (2H, m), 7.37–7.33 (2H, m), 7.23–7.16 (3H, m), 6.88 (2H, d, *J* = 7.2 Hz), 6.80 (1H, dd, *J* = 11.9, 8.7 Hz), 3.59–3.56 (1H, m), 3.33–3.27 (2H, m), 1.87 (3H, br s).

Methyl 4-((*S*)-1-(((*R*)-*tert*-butylsulfinyl)amino)-1-(2-fluorophenyl)ethyl)tetrahydro-2*H*-thiopyran-4-carboxylate (66). To a solution of diisopropylamine (12.1 mL, 86.0 mmol) in THF (80 mL) was added dropwise *n*-BuLi (1.60 M in hexane; 51.4 mL, 82.0 mmol) at –78 °C. The mixture was allowed to warm to 0 °C and stirred at the same temperature for 20 min. The mixture was cooled to –78 °C, and a solution of methyl tetrahydro-*2H*-thiopyran-4-carboxylate (9.89 g, 61.7 mmo) in THF (40 mL) was added dropwise to the mixture. After being stirred at the same temperature for 45 min, a solution of ClTi(O*i*-Pr)$_3$ (20.7 mL, 86.0 mmol) in THF (40 mL) was added dropwise at –78 °C. The mixture was stirred at the same temperature for 10 min, and then **25** (9.93 g, 41.1 mmol) in THF (40 mL) was added dropwise. After stirring for 10 min, the mixture was quenched with aqueous NH_4Cl solution. The resulting mixture was filtered through Celite and evaporated. The residue was purified by flash column chromatography (silica gel; EtOAc/hexane, gradient: 20–70% EtOAc) to give **66** (9.80 g, 59%) as a yellow solid. ^{1}H NMR (400 MHz, $CDCl_3$) δ 7.36–7.27 (2H, m), 7.12–7.08 (1H, m), 7.03 (1H, ddd, J = 13.3, 8.2, 1.1 Hz), 4.97 (1H, s), 3.77 (3H, s), 2.81–2.74 (1H, m), 2.66–2.62 (1H, m), 2.55–2.47 (4H, m), 1.91 (3H, d, J = 4.1 Hz), 1.71–1.64 (1H, m), 1.39–1.32 (1H, m).

Methyl (*S*)-4-(1-((*tert*-butoxycarbonyl)amino)-1-(2-fluorophenyl)ethyl)tetrahydro-2*H*-thiopyran-4-carboxylate (67). A mixture of **66** (9.80 g, 24.4 mmol) and HCl (4 M in 1,4-dioxane; 9.15 mL, 36.6 mmol) in MeOH (98 mL) was stirred at room temperature for 2 h. The mixture was diluted with Et_2O, and the organic layers were back extracted with H_2O. The aqueous layer was basified with K_2CO_3, and the aqueous layer was extracted with EtOAc. The organic layers were washed with water and concentrated to give the crude compound (9.36 g) as a yellow oil. A mixture of this crude compound and Boc_2O (22.5 mL, 97.0 mmol) was stirred at 50 °C for 7 h. The mixture was cooled to room temperature and carefully treated with 1-methylpiperazine (8.04 mL, 72.5 mmol). The resulting mixture was evaporated, and the residue was purified by flash column chromatography (silica gel; EtOAc/hexane, gradient: 0–10% EtOAc) to give **67** (9.03 g, 94% over 2 steps) as a white solid. ^{1}H NMR (400 MHz, $CDCl_3$) δ 7.24–7.15 (2H, m), 7.07 (1H, t, J = 7.5 Hz), 6.97 (1H, dd, J = 12.9, 8.0 Hz), 6.08 (1H, br s), 3.72 (3H, s), 2.66–2.60 (2H, m), 2.57–2.45 (3H, m), 2.30–2.25 (1H, m), 1.91 (3H, br s), 1.74–1.66 (2H, m), 1.34 (9H, br s).

***tert*-Butyl (*S*)-(1-(2-fluorophenyl)-1-(4-(hydroxymethyl)tetrahydro-2*H*-thiopyran-4-yl)ethyl)carbamate (68).** To a solution of **67** (9.03 g, 22.7 mmol) and MeOH (2.76 mL, 68.2 mmol) in THF (90 mL) was added $LiBH_4$ (3.0 M in THF; 22.7 mL, 68.2 mmol) at 0 °C. After stirring for 6 h at 50 °C, the mixture was cooled to 0 °C and quenched with aqueous NH_4Cl solution. The aqueous layer was separated and extracted with EtOAc. The organic layers were washed with water and concentrated. The residue was purified by flash column chromatography (silica gel; EtOAc/hexane, gradient: 10–100% EtOAc) to give **68** (4.04 g, 48%) as a white amorphous substance. ^1H NMR (400 MHz, $CDCl_3$) δ 7.31–7.29 (1H, m), 7.24–7.19 (1H, m), 7.09 (1H, t, *J* = 7.6 Hz), 6.99 (1H, dd, *J* = 13.1, 8.1 Hz), 3.94 (1H, d, *J* = 11.7 Hz), 3.74 (1H, d, *J* = 11.7 Hz), 2.88–2.81 (1H, m), 2.80–2.72 (1H, m), 2.47–2.43 (1H, m), 2.38–2.28 (2H, m), 1.95 (3H, d, *J* = 3.8 Hz), 1.87–1.80 (2H, m), 1.53–1.47 (1H, m), 1.33 (9H, br s).

(*S*)-*N*-((1-(2-Fluorophenyl)-1-(4-(hydroxymethyl)tetrahydro-2*H*-thiopyran-4-yl)ethyl)carbamothioyl)benzamide (69). To a solution of **68** (6.27 g, 17.0 mmol) in DCM (63mL) was added TFA (13.1 mL, 170 mmol) at room temperature. After stirring for 30 min at the same temperature, the reaction mixture was cooled to 0 °C and quenched with aqueous K_2CO_3 solution. The aqueous layer was separated and extracted with $CHCl_3$. The organic layers were dried over Na_2SO_4, filtered, and evaporated to give the crude compound (4.18 g) as a pale yellow solid. To a solution of this crude compound (3.18 g) in DCM (32 mL) was added BzNCS (2.06 mL, 15.3 mmol) at 0 °C. After stirring for 20 h at room temperature, the reaction mixture was concentrated. The residue was purified by flash column chromatography (silica gel; EtOAc/hexane, gradient: 0–30% EtOAc) to give **69** (3.90 g, 70% over 2 steps) as a yellow amorphous substance. ^{1}H NMR (400 MHz, $CDCl_3$) δ 11.84 (1H, s), 8.78 (1H, s), 7.86–7.84 (2H, m), 7.62–7.59 (1H, m), 7.52–7.48 (2H, m), 7.32–7.26 (2H, m), 7.19–7.14 (1H, m), 7.06–6.99 (1H, m), 3.99–3.89 (2H, m), 2.94–2.85 (2H, m), 2.50–2.45 (2H, m), 2.30 (3H, br s), 2.28–2.23 (1H, m), 1.91–1.89 (2H, m), 1.83 (1H, dd, J = 13.3, 3.6 Hz), 1.76–1.73 (1H, m).

(*R*)-5-(2-Fluorophenyl)-5-methyl-2,9-dithia-4-azaspiro[5.5]undec-3-en-3-amine (70). To a solution of **69** (3.90 g, 9.02 mmol) in DCM (156 mL) was added DAST (287 μL, 1.95 mmol) at room temperature. After stirring for 15 min at the same temperature, the reaction mixture was cooled to 0 °C and then poured into aqueous K_2CO_3 solution. The aqueous layer was extracted with $CHCl_3$, and the organic layers were dried over Na_2SO_4, filtered, and evaporated. The residue was purified by flash column chromatography (silica gel; EtOAc/hexane, gradient: 10–30% EtOAc) to give the compound (1.70 g) as a pale yellow amorphous substance. A mixture of this compound (1.70 g) and hydrazine monohydrate (2.18 mL, 44.8 mmol) in MeOH/THF (9.3 mL/9.3 mL) was heated to 40 °C. After stirring for 2 h at the same temperature, the reaction mixture was concentrated. The residue was purified by flash column chromatography (amino silica gel; EtOAc/hexane, gradient: 10–30% EtOAc) to give **70** (461mg, 16% over 2 steps) as a colorless oil. ^{1}H NMR (400 MHz, $CDCl_3$) δ 7.41 (1H, td, J = 8.0, 1.7 Hz), 7.25–7.21 (1H, m), 7.14–7.10 (1H, m), 6.99 (1H, ddd, J = 13.0, 8.1, 1.2 Hz), 3.05 (1H, d, J = 13.0 Hz), 2.98 (1H, d, J = 13.0 Hz), 2.88–2.75 (2H, m), 2.46–2.40 (1H, m), 2.38–2.33 (1H, m), 2.13–2.10 (1H, m), 1.84–1.70 (2H, m), 1.67 (3H, d, J = 4.8 Hz), 1.63–1.61 (1H, m).

(*R*)-3-Amino-5-(2-fluorophenyl)-5-methyl-2,9-dithia-4-azaspiro[5.5]undec-3-ene 9,9-dioxide (71). To a solution of **70** (408 mg, 1.31 mmol) in DCM (12.2 mL) was added *m*-CPBA (40% water, 743 mg, 3.02 mmol) at 0 °C. After stirring for 1 h at the same temperature, the reaction mixture was quenched with aqueous $NaHCO_3$ and $Na_2S_2O_3$ solution. The aqueous layer was extracted with $CHCl_3$, and the organic layers were dried over Na_2SO_4, filtered, and evaporated. The residue was purified by flash column chromatography (silica gel; EtOAc/hexane, gradient: 40–80% EtOAc) to give **71** (404 mg, 90%) as a white amorphous substance. ^{1}H NMR (400 MHz, $CDCl_3$) δ 7.38 (1H, td, J = 8.1, 1.6 Hz), 7.30–7.24 (1H, m), 7.17–7.13 (1H, m), 7.02 (1H, ddd, J = 13.0, 8.1, 1.2 Hz), 3.09 (1H, d, J = 13.3 Hz), 3.04–2.86 (5H, m), 2.37–2.20 (3H, m), 1.82–1.75 (1H, m), 1.72 (3H, d, J = 4.8 Hz).

(*R*)-3-Amino-5-(5-amino-2-fluorophenyl)-5-methyl-2,9-dithia-4-azaspiro[5.5]undec-3-ene 9,9-dioxide (72). To a solution of **71** (194 mg, 0.567 mmol) in TFA (918 μL) was added sulfuric acid (227 μL, 4.25 mmol) at −10 °C. After being stirred at the same temperature for 10 min, the mixture was added dropwise HNO_3 (38.0 μL, 0851 mmol). The reaction mixture was stirred at –10 °C for 25 min and then poured into aqueous K_2CO_3 solution. The aqueous layer was separated and extracted with EtOAc. The organic layers were washed with water and evaporated to give the crude compound (214 mg) as a white amorphous substance. A suspension of this crude compound, Fe (247 mg, 4.42 mmol), and NH_4Cl (355 mg, 6.64 mmol) in toluene/H_2O (4.3 mL/4.3 mL) was stirred at 80 °C for 1 h. The mixture was cooled to room temperature and quenched with aqueous K_2CO_3 solution and filtered through Celite. The aqueous layer was treated with NaCl and extracted with $CHCl_3$. The organic layers were dried over Na_2SO_4, filtered, and evaporated. The residue was purified twice by flash column chromatography (amino silica gel; EtOAc/hexane, gradient: 80–100% EtOAc then 20% MeOH in EtOAc) to give **72** (156 mg, 77% over 2 steps) as a pale yellow oil. ^{1}H NMR (400 MHz, $CDCl_3$) δ 6.81 (1H, dd, J = 12.4, 8.5 Hz), 6.65 (1H, dd, J = 6.7, 2.9 Hz), 6.58–6.54 (1H, m), 3.55 (2H, s), 3.08 (1H, d, J = 13.3 Hz), 3.03–2.88 (5H, m), 2.39–2.16 (3H, m), 1.80 (1H, dd, J = 15.1, 3.1 Hz), 1.68 (3H, d, J = 4.6 Hz).

Biochemical BACE1 Assay. The biochemical BACE1 IC_{50} values were determined by a FRET assay using an APP derived peptide as described previously.[9h]

Cellular Aβ Assay. The cellular Aβ IC_{50} values were determined by measuring Aβ42 using a sandwich AlphaLISA assay in SKNBE2 cells expressing the wild-type APP as described previously.[9h]

Biochemical BACE2 Assay. BACE2 enzymatic activity was assessed by FRET assay using an amyloid precursor protein (APP) derived 13-amino acid peptide that contains the "Swedish" Lys-Met/Asn-Leu mutation of the APP β-secretase cleavage site as a substrate (Bachem catalogue no. M-2465) and soluble BACE2 in a final concentration of 0.4 μg/mL. This substrate contains two fluorophores; (7-methoxycoumarin-4-yl) acetic acid (Mca) is a fluorescent donor with excitation wavelength at 320 nm and emission at 405 nm and 2,4-dinitrophenyl (Dnp) is a proprietary quencher acceptor. The increase in fluorescence is linearly related to the rate of proteolysis. In a 384-well format, BACE2 was incubated with the substrate and the inhibitor. The amount of proteolysis was directly measured by fluorescence measurement in a Fluoroskan microplate fluorometer (Thermo Scientific). For the low control, no enzyme was added to the reaction mixture.

Biochemical Radioligand Binding Assay for BACE1 and BACE2. The binding affinity (K_i) of compounds under investigation to either BACE1 or BACE2 was determined in a competitive radioligand binding assay, i.e., in competition with the tritiated non-selective BACE1/BACE 2 inhibitor [^{3}H]-JNJ-962 (JNJ-962 (CAS#: 1397684-09-1): BACE1 K_i = 0.69 nM, BACE2 K_i = 0.29 nM). Briefly, in test tubes, compounds of interest were combined with the radioligand and the BACE1 or BACE2-expressing HEK293 derived membranes. The competitive binding reaction was performed at pH 6.2 and incubated at room temperature until the equilibrium was reached. Afterwards free radioligand was separated from bound radioligand by filtration with a Brandell 96 harvester. The filter was washed, filter sheets were punched into scintillation vials, and Ultima Gold scintillation cocktail was added. The day after, the vials were counted in a Tricarb scintillation counter to obtain the disintegrations per minute (dpm) of the bound radioligand. Calculating the %Inhibition = 100- [(sample-LC)/(HC-LC))*100], with HC being the high control, i.e. total binding of radioligand and LC representing the non-specific binding measured in the presence of 10 μM of a known BACE inhibitor, allowed to fit curves through the data points of the different doses of the test compound. The pIC_{50} or IC_{50} is calculated and can be converted to K_i by the formula $K_i = IC_{50}/(1+([RL]/K_d))$, with [RL] being the concentration of the radioligand and K_d the determined dissociation constant of the radioligand-membrane complex.

P-gp Assay. The P-gp efflux ratios (ER) were determined in LLC-PK1 cells transfected with human MDR1, and the permeability coefficients (P_{app}) were determined in wild-type LLC-PK1 cells as described previously.[27c]

Metabolic Stability Assay. The metabolic stability in human and mouse microsomes was determind as described previously.[27b]

PK/PD Study in Wild-Type Mice. All animal studies were performed with the approval of the Shionogi Animal Care and Use Committee. Male ICR mice (n = 4) were dosed po with the compound dissolved in 20% HPBCD. The detailed method was descrived previously.[27c]

ASSOCIATED CONTENT

Supporting Information.

The Supporting Information is available free of charge on the ACS publication website at DOI: ~.

Experimental procedures and charanterization data for compounds **15**, **18**, **19**, **20**, and **21**, NOE for compounds **44** and **45**, synthesis of [^{3}H]-JNJ-962, and crystallographic data (PDF).

SMILE strings, BACE1 IC_{50}, BACE2 IC_{50}, and cellular Aβ42 IC_{50} (CSV).

Accession Codes

8 bound to BACE1: 6JSG; **16** bound to BACE1: 6JSE; **17** bound to BACE1: 6JSF; **22** bound to BACE1: 6JSN; and **22** bound to BACE2: 6JSZ.

AUTHOR INFORMATION

Corresponding Author

*Phone: +81-6-6331-6190. Fax: +81-6-6332-6385. E-mail: ken-ichi.kusakabe@shionogi.co.jp.

ORCID

Harrie. J. M. Gijsen: 0000-0001-8020-4848

Ken-ichi Kusakabe: 0000-0001-9055-8267

Author Contributions

#These authors contributed equally to this paper.

Present Addresses

┴API Process Development Department (Biotechnology), Pharmaceutical Technology Division, Chugai Pharmaceutical Co., Ltd, 5-1, Ukima 5-chome, Kita-ku, Tokyo, 115-8543 Japan

Notes

The authors declare no competing financial interest.

ACKNOWLEDGMENTS

We thank Ronghui Lin for the synthesis of [^{3}H]-JNJ-962, Stefan Steinbacher (Proteros) for the BACE2 X-ray crystallography, Maki Hattori, Masanori Nakae, and Maito Douma for the biological assays, Shun Noritake for the HRMS analysis, and Yukiko Kan for the NMR analysis. We gratefully thank the members of the Janssen-Shionogi research collaboration for the support of this program. We are grateful to Judy Noguchi for proofreading the manuscript.

ABBREVIATIONS

AD, Alzheimer's disease; Aβ, amyloid β; APP, amyloid precursor protein; BACE1, β-site amyloid precursor protein cleaving enzyme 1; BzNCS, benzoyl isothiocyanate; DAST, *N*,*N*-diethylaminosulfur trifluoride; DIAN, the Dominantly Inherited Alzheimer Network; EDC, 1-ethyl-3-(3-dimethylaminopropyl)carbodiimide; FRET, fluorescence resonance energy transfer; HATU, 1-[bis(dimethylamino)methylene]-1*H*-1,2,3-triazolo[4,5-*b*]pyridinium 3-oxide hexafluorophosphate; HLM, human liver microsome; HPBCD, 2-hydroxypropyl-β-cyclodextrin; *m*-CPBA, *m*-chloroperoxybenzoic acid; MDR, multidrug resistance; MLM, mouse liver microsome; PET, positron-emission tomography; PD, pharmacodynamics; P-gp, P-glycoprotein; PK, pharmacokinetics; PMEL, pigment cell-specific melanocyte protein; TMEM27, transmembrane protein 27.

REFERENCES

(1) Prince, M.; Comas-Herrera, A.; Knapp, M.; Guerchet, M.; Karagiannidou, M. World Alzheimer Report 2016. https://www.alz.co.uk/research/WorldAlzheimerReport2016.pdf (accessed February 20, 2018).

(2) Alzheimer's Association. 2017 Alzheimer's Disease Facts and Figures. https://www.alz.org/documents_custom/2017-facts-and-figures.pdf (accessed February 20, 2018)

(3) Chancellor, D.; Dube, S.; Huntley, C. Alzheimer's disease. Ref Code: DMKC4740.

(4) Yan, R.; Vassar, R. Targeting the β secretase BACE1 for Alzheimer's disease therapy. *Lancet Neurol.* **2014**, *13*, 319–329.

(5) (a) Hardy, J.; Selkoe, D. J. The amyloid hypothesis of Alzheimer's disease: Progress and problems on the road to therapeutics. *Science* **2002**, *297*, 353–356. (b) Karran, E.; Mercken, M.; De Strooper, B. The amyloid cascade hypothesis for Alzheimer's disease: an appraisal for the development of therapeutics. *Nat. Rev. Drug Discovery* **2011**, *10*, 698–712.

(6) (a) Vassar, R.; Bennett, B. D.; Babu-Khan, S.; Kahn, S.; Mendiaz, E. A.; Denis, P.; Teplow, D. B.; Ross, S.; Amarante, P.; Loeloff, R.; Luo, Y.; Fisher, S.; Fuller, J.; Edenson, S.; Lile, J.; Jarosinski, M. A.; Biere, A. L.; Curran, E.; Burgess, T.; Louis, J.-C.; Collins, F.; Treanor, J.; Rogers, G.; Citron, M. β-Secretase cleavage of Alzheimer's amyloid precursor protein by the transmembrane aspartic protease BACE. *Science* **1999**, *286*, 735–741. (b) Sinha, S.; Anderson, J. P.; Barbour, R.; Basi, G. S.; Caccavello, R.; Davis, D.; Doan, M.; Dovey, H. F.; Frigon, N.; Hong, J.; Jacobson-Croak, K.; Jewett, N.; Keim, P.; Knops, J.; Lieberburg, I.; Power, M.; Tan, H.; Tatsuno, G.; Tung, J.; Schenk, D.; Seubert, P.; Suomensaari, S. M.; Wang, S.; Walker, D.; Zhao, J.; McConlogue, L.; John, V. Purification and cloning of amyloid precursor protein β-secretase from human brain. *Nature* **1999**, *402*, 537–540. (c) Hussain, I.; Powell, D.; Howlett, D. R.; Tew, D. G.; Meek, T. D.; Chapman, C.; Gloger, I. S.; Murphy, K. E.; Southan, C. D.; Ryan, D. M.; Smith, T. S.; Simmons, D. L.; Walsh, F. S.; Dingwall, C.; Christie, G. Identification of a novel aspartic protease (Asp 2) as β-secretase.

Mol. Cell. Neurosci. **1999**, *14*, 419–427. (d) Yan, R.; Bienkowski, M. J.; Shuck, M. E.; Miao, H.; Tory, M. C.; Pauley, A. M.; Brashler, J. R.; Stratman, N. C.; Mathews, W. R.; Buhl, A. E.; Carter, D. B.; Tomasselli, A. G.; Parodi, L. A.; Heinrikson, R. L.; Gurney, M. E. Membrane-anchored aspartyl protease with Alzheimer's disease β-secretase activity. *Nature* **1999**, *402*, 533–537. (e) Lin, X.; Koelsch, G.; Wu, S.; Downs, D.; Dashti, A.; Tang, J. Human aspartic protease memapsin 2 cleaves the β-secretase site of β-amyloid precursor protein. *Proc. Natl. Acad. Sci. U. S. A.* **2000**, *97*, 456–1460.

(7) (a) Ghosh, A. K.; Osswald, H. L. BACE1 (β-secretase) inhibitors for the treatment of Alzheimer's disease. *Chem. Soc. Rev.* 2014, 43, 6765–6813. (b) Yuan, J.; Venkatraman, S.; Zheng, Y.; McKeever, B. M.; Dillard, L. W.; Singh, S. B. Structure based design of β-site APP cleaving enzyme 1 (BACE) inhibitors for the treatment of Alzheimer's disease. disease. *J. Med. Chem.* **2013**, *56*, 4156–4180.

(8) (a) Oehlrich, D.; Prokopcova, H.; Gijsen, H. J. M. The evolution of amidine-based brain penetrant BACE1 inhibitors. *Bioorg. Med. Chem. Lett.* **2014**, *24*, 2033–2045. (b) Hall, A.; Gijsen, H. J. M. Targeting β-secretase (BACE) for the treatment of Alzheimer's disease. In *Comprehensive Medicinal Chemistry III*, 3rd ed.; Chackalamannil, S., Rotella, D. P., Ward, S. E., Eds.; Elsevier: Oxford, 2017; vol. 7, pp 326–383. (c) Hsiao, C.-C.; Rombouts, F.; Gijsen, H. J. M. New evolutions in the BACE1 inhibitor field from 2014 to 2018. *Bioorg. Med. Chem. Lett.* DOI: 10.1016/j.bmcl.2018.12.049.

(9) (a) Huang, H.; La, D. S.; Cheng, A. C.; Whittington, D. A.; Patel, V. F.; Chen, K.; Dineen, T. A.; Epstein, O.; Graceffa, R.; Hickman, D.; Kiang, Y.-H.; Louie, S.; Luo, Y.; Wahl, R. C.; Wen, P. H.; Wood, S.; Fremeau, R. T. Structure- and property-based design of aminooxazoline xanthenes as selective, orally efficacious, and CNS penetrable BACE inhibitors for the treatment of alzheimer's disease. *J. Med. Chem.* **2012**, *55*, 9156–9169. (b) Swahn, B.-M.; Kolmodin, K.; Karlstroem, S.; von Berg, S.; Soederman, P.; Holenz, J.; Berg, S.; Lindstroem, J.; Sundstroem, M.; Turek, D.; Kihlstroem, J.; Slivo, C.; Andersson, L.; Pyring, D.; Rotticci, D.; Oehberg, L.; Kers, A.; Bogar, K.; Bergh, M.; Olsson, L.-L.; Janson, J.; Eketjaell, S.; Georgievska, B.; Jeppsson, F.; Faelting, J. Design and synthesis of β-site amyloid precursor protein cleaving enzyme (BACE1) inhibitors with in vivo brain reduction of β-amyloid peptides. *J. Med. Chem.* **2012**, *55*, 9346–9361. (c) Mandal, M.; Zhu, Z.; Cumming, J. N.; Liu, X.; Strickland, C.; Mazzola, R. D.; Caldwell, J. P.; Leach, P.; Grzelak, M.; Hyde, L.; Zhang, Q.; Terracina, G.; Zhang, L.; Chen, X.; Kuvelkar, R.; Kennedy, M. E.; Favreau, L.; Cox, K.; Orth, P.; Buevich, A.; Voigt, J.; Wang, H.; Kazakevich, I.; McKittrick, B. A.; Greenlee, W.; Parker, E. M.; Stamford, A. W. Design and validation of bicyclic iminopyrimidinones as beta amyloid cleaving enzyme-1 (BACE1) inhibitors: Conformational constraint to favor a bioactive conformation. *J. Med. Chem.* **2012**, *55*, 9331–9345. (d) Hunt, K. W.; Cook, A. W.; Watts, R. J.; Clark, C. T.; Vigers, G.; Smith, D.; Metcalf, A. T.; Gunawardana, I. W.; Burkard, M.; Cox, A. A.; Geck D., Mary K.; Dutcher, D.; Thomas, A. A.; Rana, S.; Kallan, N. C.; DeLisle, R. K.; Rizzi, J. P.; Regal, K.; Sammond, D.; Groneberg, R.; Siu, M.; Purkey, H.; Lyssikatos, J. P.; Marlow,

A.; Liu, X.; Tang, T. P. Spirocyclic β-site amyloid precursor protein cleaving enzyme 1 (BACE1) inhibitors: From hit to lowering of cerebrospinal fluid (CSF) amyloid β in a higher species. *J. Med. Chem.* **2013**, *56*, 3379–3403. (e) Dineen, T. A.; Chen, K.; Cheng, A. C.; Derakhchan, K.; Epstein, O.; Esmay, J.; Hickman, D.; Kreiman, C. E.; Marx, I. E.; Wahl, R. C.; Wen, P. H.; Weiss, M. M.; Whittington, D. A.; Wood, S.; Fremeau, R. T.; White, R. D.; Patel, V. F. Inhibitors of β-site amyloid precursor protein cleaving enzyme (BACE1): Identification of (*S*)-7-(2-fluoropyridin-3-yl)-3-((3-methyloxetan-3-yl)ethynyl)-5'H-spiro[chromeno[2,3-b]pyridine-5,4'-oxazol]-2'-amine (AMG-8718). *J. Med. Chem.* **2014**, *57*, 9811–9831. (f) Brodney, M. A.; Beck, E. M.; Butler, C. R.; Barreiro, G.; Johnson, E. F.; Riddell, D.; Parris, K.; Nolan, C. E.; Fan, Y.; Atchison, K.; Gonzales, C.; Robshaw, A. E.; Doran, S. D.; Bundesmann, M. W.; Buzon, L.; Dutra, J.; Henegar, K.; LaChapelle, E.; Hou, X.; Rogers, B. N.; Pandit, J.; Lira, R.; Martinez-Alsina, L.; Mikochik, P.; Murray, J. C.; Ogilvie, K.; Price, L.; Sakya, S. M.; Yu, A.; Zhang, Y.; O'Neill, B. T. Utilizing structures of CYP2D6 and BACE1 complexes to reduce risk of drug-drug interactions with a novel series of centrally efficacious BACE1 inhibitors. *J. Med. Chem.* **2015**, *58*, 3223–3252. (g) Wu, Y.-J.; Guernon, J.; Yang, F.g; Snyder, L.; Shi, J.; McClure, A.; Rajamani, R.; Park, H.; Ng, A.; Lewis, H.; Chang, C. Y.; Camac, D.; Toyn, J. H.; Ahlijanian, M. K.; Albright, C. F.; Macor, J. E.; Thompson, L. A. Targeting the BACE1 active site flap leads to a potent inhibitor that elicits robust brain Aβ reduction in rodents. *ACS Med. Chem. Lett.* **2016**, *7*, 271–276. (h) Rombouts, F. J. R.; Tresadern, G.; Delgado, O.; Martinez-Lamenca, C.; Van Gool, M.; Garcia-Molina, A.; Alonso de Diego, S. A.;

Oehlrich, D.; Prokopcova, H.; Alonso, J. M.; Austin, N.; Borghys, H.; Van Brandt, S.; Surkyn, M.; De Cleyn, M.; Vos, A.; Alexander, R.; Macdonald, G.; Moechars, D.; Gijsen, H.; Trabanco, A. A. 1,4-Oxazine β-secretase 1 (BACE1) inhibitors: From hit generation to orally bioavailable brain penetrant leads. *J. Med. Chem.* **2015**, *58*, 8216–8235. (i) Neumann, U.; Schmid, P.; Shimshek, D. R.; Staufenbiel, M.; Jacobson, L. H; Rueeger, H.; Machauer, R.; Veenstra, S. J.; Lueoend, R. M; Tintelnot-Blomley, M.; Laue, G.; Beltz, K.; Vogg, B.; Schmid, P.; Frieauff, W.; Staufenbiel, M.; Jacobson, L. H. A novel BACE inhibitor NB-360 shows a superior pharmacological profile and robust reduction of amyloid-β and neuroinflammation in APP transgenic mice. *Mol. Neurodegener.* **2015**, *10*, 44.

(10) (a) Scott, J. D.; Li, S. W.; Brunskill, A. P. J.; Chen, X.; Cox, K.; Cumming, J. N.; Forman, M.; Gilbert, E. J.; Hodgson, R. A.; Hyde, L. A.; Jiang, Q.; Iserloh, U.; Kazakevich, I.; Kuvelkar, R.; Mei, H.; Meredith, J.; Misiaszek, J.; Orth, P.; Rossiter, L. M.; Slater, M.; Stone, J.; Strickland, C. O.; Voigt, J. H.; Wang, G.; Wang, H.; Wu, Y.; Greenlee, W. J.; Parker, E. M.; Kennedy, M. E.; Stamford, A. W. Discovery of the 3-imino-1,2,4-thiadiazinane 1,1-dioxide derivative verubecestat (MK-8931)–A β-site amyloid precursor protein cleaving enzyme 1 inhibitor for the treatment of Alzheimer's disease *J. Med. Chem.* **2016**, *59*, 10435–10450. (b) Kennedy M. E.; Chen X.; Hodgson R. A.; Hyde L. A.; Kuvelkar R.; Parker E. M; Stamford A. W.; Cumming J. N.; Li W.; Scott J. D.; Cox K.; Dockendorf M. F.; Kleijn H. J.; Mei H.; Stone J. A.; Egan M.; Ereshefsky L.; Jhee S.;

Mattson B. A.; Palcza J.; Tanen M.; Troyer M. D.; Tseng J. L.; Forman M. S. The BACE1 inhibitor verubecestat (MK-8931) reduces CNS β-amyloid in animal models and in Alzheimer's disease patients. *Sci. Transl. Med.* **2016**, *8*, 363ra150. (c) Cumming, J. N.; Scott, J. D.; Strickland, C. O. Verubecestat. In *Comprehensive Medicinal Chemistry III*, 3rd ed.; Chackalamannil, S., Rotella, D. P., Ward, S. E., Eds.; Elsevier: Oxford, 2017; vol. 8, pp 204–251. (d) Egan, M. F.; Kost, J.; Tariot, P. N.; Aisen, P. S.; Cummings, J. L.; Vellas, B.; Sur, C.; Mukai, Y.; Voss, T.; Furtek, C.; Mahoney, E.; Mozley, L. H.; Vandenberghe, R.; Mo, Y.; Michelson, D. Randomized trial of verubecestat for mild-to-moderate Alzheimer's disease. *N. Engl. J. Med.* **2018**, *378*, 1691–1703.

(11) (a) Alzforum. http://www.alzforum.org/therapeutics/elenbecestat (accessed July 24, 2017) (b) Suzuki, Y.; Motoki, T.; Kaneko, T.; Takaishi, M.; Ishida, T.; Takeda, K.; Kita, Y.; Yamamoto, N.; Khan, A.; Dimopoulos, P. Preparation of Condensed Aminodihydrothiazine Derivatives as Inhibitors of β-Site APP-cleaving Enzyme 1 (BACE1). WO 2009091016 A1, July 23, 2009.

(12) (a) Eketjaell, S.; Janson, J.; Kaspersson, K.; Bogstedt, A.; Jeppsson, F.; Faelting, J.; Haeberlein, S. B.; Kugler, A. R.; Alexander, R. C.; Cebers, G.; Ho, P. AZD3293: A novel, orally active BACE1 inhibitor with high potency and permeability and markedly slow off-rate kinetics. *J. Alzheimers Dis.* **2016**, *50*, 1109–1123. (b) Alzforum. https://www.alzforum.org/therapeutics/azd3293 (accessed December 23, 2018)

(13) Neumann, U.; Ufer, M.; Jacobson, L. H.; Rouzade-Dominguez, M.-L.; Huledal, G.; Kolly, C.; Lueoend, R. M.; Machauer, R.; Veenstra, S. J.; Hurth, K.; Rueeger, H.; Tintelnot-Blomley, M.; Staufenbiel, M.; Shimshek, D. R.; Perrot, L.; Frieauff, W.; Dubost, V.; Schiller, H.; Vogg, B.; Beltz, K.; Avrameas, A.; Kretz, S.; Pezous, N.; Rondeau, J.; Beckmann, N.; Hartmann, A.; Vormfelde, S.; David, O. J.; Galli, B.; Ramos, R.; Graf, A.; Lopez Lopez, C. The BACE-1 inhibitor CNP520 for prevention trials in Alzheimer's disease. *EMBO Mol. Med.* **2018**, *10*, e9316.

(14) (a) Timmers, M.; Van Broeck, B.; Ramael, S.; Slemmon, J.; De Waepenaert, K.; Russu, A.; Bogert, J.; Stieltjes, H.; Shaw, L. M.; Engelborghs, S.; Moechars, D.; Mercken, M.; Liu, E.; Sinha, V.; Kemp, J.; Van Nueten, L.; Tritsmans, L.; Streffer, J. R. Profiling the dynamics of CSF and plasma Aβ reduction after treatment with JNJ-54861911, a potent oral BACE inhibitor. *Alzheimers Dement (N Y)* **2016**, *2*, 201–212. (b) The Janssen Pharmaceutical Campanies of Johnson & Johnson. https://www.janssen.com/ja/node/45771 (accessed December 23, 2018)

(15) Bateman, R. J.; Xiong, C.; Benzinger, T. L. S.; Fagan, A. M.; Goate, A.; Fox, N. C.; Marcus, D. S.; Cairns, N. J.; Xie, X.; Blazey, T. M.; Holtzman, D. M.; Santacruz, A.; Buckles, V.; Oliver, A.; Moulder, K.; Aisen, P. S.; Ghetti, B.; Klunk, W. E.; McDade, E.; Martins, R. N.; Masters, C. L.; Mayeux, R.; Ringman, J. M.; Rossor, M. N.; Schofield, P. R.; Sperling, R. A.; Salloway, S.; Morris, J. C.; Dominantly Inherited Alzheimer Network.

Clinical and biomarker changes in dominantly inherited Alzheimer's disease. *N. Engl. J. Med.* **2012**, *367*, 795–804.

(16) Villemagne, Victor L.; Burnham, Samantha; Bourgeat, Pierrick; Brown, Belinda; Ellis, Kathryn A.; Salvado, Olivier; Szoeke, Cassandra; Macaulay, S. Lance; Martins, Ralph; Maruff, Paul; Ames, David; Rowe, Christopher C.; Masters, C. L. Amyloid β deposition, neurodegeneration, and cognitive decline in sporadic Alzheimer's disease: a prospective cohort study. *Lancet Neurol.* **2013**, *12*, 357–367.

(17) (a) Salloway, S.; Sperling, R.; Fox, N. C.; Blennow, K.; Klunk, W.; Raskind, M.; Sabbagh, M.; Honig, L. S.; Porsteinsson, A. P.; Ferris, S.; Reichert, M.; Ketter, N.; Nejadnik, B.; Guenzler, V.; Miloslavsky, M.; Wang, D.; Lu, Y.; Lull, J.; Tudor, I. C.; Liu, E.; Grundman, M.; Yuen, E.; Black, R.; Brashear, H. R. Two phase 3 trials of bapineuzumab in mild-to-moderate Alzheimer's disease. *N. Engl. J. Med.* **2014**, *370*, 322–333. (b) Doody, R. S.; Thomas, R. G.; Farlow, M.; Iwatsubo, T.; Vellas, B.; Joffe, S.; Kieburtz, K.; Raman, R.; Sun, X.; Aisen, P. S.; Siemers, E.; Liu-Seifert, H.; Mohs, R. Phase 3 trials of solanezumab for mild-to-moderate Alzheimer's disease. *N. Engl. J. Med.* **2014**, *370*, 311–321. (c) https://www.alzforum.org/news/research-news/merck-pulls-plug-phase-23-bace-inhibitor-trial (accessed December 23, 2018)

(18) (a) Sperling, R.; Mormino, E.; Johnson, K. The evolution of preclinical Alzheimer's disease: implications for prevention trials. *Neuron* **2014**, *84*, 608–622. (b) Jack, C. R.;

Knopman, D. S.; Jagust, W. J.; Petersen, R. C.; Weiner, M. W.; Aisen, P. S.; Shaw, L. M.; Vemuri, P.; Wiste, H. J.; Weigand, S. D.; Lesnick, T. G.; Pankratz, V. S.; Donohue, M. C.; Trojanowski, J. Q. Tracking pathophysiological processes in Alzheimer's disease: an updated hypothetical model of dynamic biomarkers *Lancet Neurol.* **2013**, *12*, 207–216.

(19) Farzan, M.; Schnitzler, C. E.; Vasilieva, N.; Leung, D.; Choe, H. BACE2, a β-secretase homolog, cleaves at the β site and within the amyloid-β region of the amyloid-β precursor protein. *Proc. Natl. Acad. Sci. U. S. A.* **2000**, *97*, 9712–9717.

(20) Esterhazy, D.; Stuetzer, I.; Wang, H.; Rechsteiner, M. P.; Beauchamp, J.; Doebeli, H.; Hilpert, H.; Matile, H.; Prummer, M.; Schmidt, A.; Lieske, N.; Boehm, B.; Marselli, L.; Bosco, D.; Kerr-Conte, J.; Aebersold, .; Spinas, G. A.; Moch, H.; Migliorini, C.; Stoffel, M. Bace2 ts a β cell-enriched protease that regulates pancreatic β cell function and mass. *Cell Metab.* **2011**, *14*, 365–377.

(21) Rochin L.; Hurbain I.; Serneels L.; Fort C.; Watt B.; Leblanc P.; Marks M. S; De Strooper, B.; Raposo G.; van Niel, G. BACE2 processes PMEL to form the melanosome amyloid matrix in pigment cells. *Proc. Natl. Acad. Sci. U. S. A.* **2013**, *110*, 10658–10663.

(22) Shimshek, D. R.; Jacobson, L. H.; Kolly, C.; Zamurovic, N.; Balavenkatraman, K. K.; Morawiec, L.; Kreutzer, R.; Schelle, J.; Jucker, M.; Bertschi, B.; Theil, D.; Heier, A.; Bigot, K.; Beltz, K.; Machauer, R.; Brzak, I.; Perrot, L.; Neumann, U. Pharmacological BACE1

and BACE2 inhibition induces hair depigmentation by inhibiting PMEL17 processing in mice. *Sci. Rep.* **2016**, *6*, 21917.

(23) (a) Ostermann, Nils; Eder, Joerg; Eidhoff, Ulf; Zink, Florence; Hassiepen, Ulrich; Worpenberg, Susanne; Maibaum, Juergen; Simic, Oliver; Hommel, Ulrich; Gerhartz, Bernd. Crystal structure of human BACE2 in complex with a hydroxyethylamine transition-state inhibitor. *J. Mol. Biol.* **2006**, *355*, 249–261. (b) Banner D. W; Gsell B.; Benz J.; Bertschinger J.; Burger D.; Brack S.; Cuppuleri S.; Debulpaep M.; Gast A.; Grabulovski D.; Hennig M.; Hilpert H.; Huber W.; Kuglstatter A.; Kusznir E.; Laeremans T.; Matile H.; Miscenic C.; Rufer A. C; Schlatter D.; Steyaert J.; Stihle M.; Thoma R.; Weber M.; Ruf A. Mapping the conformational space accessible to BACE2 using surface mutants and cocrystals with Fab fragments, Fynomers and Xaperones. *Acta. Crystallogr. D Biol. Crystallogr.* **2013**, *69*, 1124–1137.

(24) (a) Patel, S.; Vuillard, L.; Cleasby, A.; Murray, C. W.; Yon, J. Apo and inhibitor complex Structures of BACE (β-secretase). *J. Mol. Biol.* **2004**, *343*, 407–416. (b) Hong, L.; Tang, J. Flap position of free Memapsin 2 (β-secretase), a model for flap opening in aspartic protease catalysis. *Biochemistry* **2004**, *43*, 4689–4695.

(25) Malamas, M. S.; Barnes, K.; Johnson, M.; Hui, Y.; Zhou, P.; Turner, J.; Hu, Y.; Wagner, E.; Fan, K.; Chopra, R.; Olland, A.; Bard, J.; Pangalos, M.; Reinhart, P.;

Robichaud, A. J. Di-substituted pyridinyl aminohydantoins as potent and highly selective human β-secretase (BACE1) inhibitors. *Bioorg. Med. Chem.* **2010**, *18*, 630–639.

(26) (a) Brodney, M. A.; Beck, E. M.; Butler, C. R.; Zhang, L.; O'Neill, B. T.; Barreiro, G.; Lachapelle, E. A.; Rogers, B. N. Preparation of *N*-(2-Amino-6-methyl-4,4*a*,5,6-tetrahydropyrano[3,4-*d*][1,3]thiazin-8*a*(8*h*)-yl-1,3-thiazol-4-yl) Amides as Inhibitors of Beta-site Amyloid Precursor Protein Cleaving Enzyme 1 (BACE1). WO 2015155626 A1, October 15, 2015. (b) Richards, S. J.; Hembre, E. J.; Lopez, J. E.; Winneroski, L. L., Jr.; Woods, T. A.; Mcmahon, J. A. Preparation of 2-Amino-5-(1,1-difluoroalkyl)-4,4*a*,5,7-tetrahydrofuro[3,4-*d*][1,3]thiazin-7*a*-yl]-4-fluorophenyl]-5-(1,2,4-triazol-1-yl)pyrazine-2-carboxamides as Selective BACE1 Inhibitors. US 20160244465 A1, August 25, 2016. (c) Allen, J. R.; Amegadzie, A.; Bourbeau, M. P.; Brown, J. A.; Chen, N.; Frohn, M. J.; Liu, L.; Liu, Q.; Pettus, L. H.; Qian, W.; Reeves, C. M.; Siegmund, A. C. Preparation of Vinyl Fluoride Cyclopropyl Fused Thiazin-2-amine Compounds as Beta-secretase Inhibitors and Methods of Use. WO 2017024180 A1, February 9, 2017. (d) O'Neill, B. T.; Beck, E. M.; Butler, C. R.; Nolan, C. E.; Gonzales, C.; Zhang, L.; Doran, S. D.; Lapham, K.; Buzon, L. M.; Dutra, J. K.; Barreiro, G.; Hou, X.; Martinez-Alsina, L. A.; Rogers, B. N.; Villalobos, A.; Murray, J. C.; Ogilvie, K.; La Chapelle, E. A.; Chang, C.; Lanyon, L. F.; Steppan, C. M.; Robshaw, A.; Hales, K.; Boucher, G. G.; Pandher, K.; Houle, C.; Ambroise, C. W.; Karanian, D.; Riddell, D.; Bales, K. R.; Brodney, M. A. Design and synthesis of clinical candidate PF-06751979: A potent, brain penetrant, β-site amyloid precursor protein

cleaving enzyme 1 (BACE1) inhibitor lacking hypopigmentation. *J. Med. Chem.* **2018**, *61*, 4476–4504. (e) Johansson, P.; Kaspersson, K.; Gurrell, I. K.; Baeck, E.; Eketjaell, S.; Scott, C. W.; Cebers, G.; Thorne, P.; McKenzie, M. J.; Beaton, H.; Davey, P.; Kolmodin, K.; Holenz, J.; Duggan, M. E.; Budd H., Samantha; Burli, R. W. Toward β-secretase-1 inhibitors with improved isoform selectivity. *J. Med. Chem.* **2018**, 61(8), 3491-3502.

(27) (a) Kobayashi, N.; Ueda, K.; Itoh, N.; Suzuki, S.; Sakaguchi, G.; Kato, A.; Yukimasa, A.; Hori, A.; Koriyama, Y.; Haraguchi, H.; Yasui, K.; Kanda, Y. Preparation of 2-aminodihydrothiazine derivatives as β-secretase inhibitors. WO 2007049532 A1, March 3, 2007. (b) Fuchino, K.; Mitsuoka, Y.; Masui, M.; Kurose, N.; Yoshida, S.; Komano, K.; Yamamoto, T.; Ogawa, M.; Unemura, C.; Hosono, M.; Ito, H.; Sakaguchi, G.; Ando, S.; Ohnishi, S.; Kido, Y.; Fukushima, T.; Miyajima, H.; Hiroyama, S.; Koyabu, K.; Dhuyvetter, D.; Borghys, H.; Gijsen, H. J. M.; Yamano, Y.; Iso, Y.; Kusakabe, K.-I. Rational design of novel 1,3-oxazine based β-secretase (BACE1) inhibitors: Incorporation of a double bond to reduce P-gp efflux leading to robust Aβ reduction in the brain. *J. Med. Chem.* **2018**, *61*, 5122–5137. (c) Nakahara, K.; Fuchino, K.; Komano, K.; Asada, N.; Tadano, G.; Hasegawa, T.; Yamamoto, T.; Sako, Y.; Ogawa, M.; Unemura, C.; Hosono, M.; Ito, H.; Sakaguchi, G.; Ando, S.; Ohnishi, S.; Kido, Y.; Fukushima, T.; Dhuyvetter, D.; Borghys, H.; Gijsen, H. J. M.; Yamano, Y.; Iso, Y.; Kusakabe, K.-I. Discovery of potent and centrally active 6-substituted 5-fluoro-1,3-dihydro-oxazine β-secretase (BACE1) inhibitors via active conformation stabilization. *J. Med. Chem.* **2018**, *61*, 5525–5546. (d)

Oguma, T.; Anan, K.; Suzuki, S.; Hisakawa, S.; Takada, A.; Ogawa, M.; Kusakabe, K.-I. Synthesis of a 6-CF_3-substituted 2-amino-dihydro-1,3-thiazine b-secretase inhibitor by *N,N*-diethylsulfur trifluoride-mediated chemoselective cyclization. *J. Org. Chem.* **2019**, *84*, 4893–4897.

(28) Hilpert, H.; Guba, W.; Woltering, T. J.; Wostl, W.; Pinard, E.; Mauser, H.; Mayweg, A. V.; Rogers-Evans, M.; Humm, R.; Krummenacher, D.; Muser, T.; Schnider, C.; Jacobsen, H.; Ozmen, L.; Bergadano, A.; Banner, D. W.; Hochstrasser, R.; Kuglstatter, A.; David-Pierson, P.; Fischer, H.; Polara, A.; Narquizian, R. β-Secretase (BACE1) inhibitors with high in vivo efficacy suitable for clinical evaluation in Alzheimer's disease *J. Med. Chem.* **2013**, *56*, 3980–3995.

(29) Trabanco-Suarez, Andres Avelino; Gijsen, Henricus Jacobus Maria; Van Gool, Michiel Luc Maria; Vega Ramiro, Juan Antonio; Delgado-Jimenez, Francisca. Preparation of Dihydropyrazolopyrazinylamine Derivatives for Use as β-Secretase Inhibitors. WO 2012117027 A1, September 7, 2012.

(30) The cocrystal structure was obtained at Proteros. http://www.proteros.de/ (accessed September 10, 2017)

(31) Kobayashi, N.; Ueda, K.; Itoh, N.; Suzuki, S.; Sakaguchi, G.; Kato, A.; Yukimasa, A.; Hori, A.; Kooriyama, Y.; Haraguchi, H.; Yasui, K.; Kanda, Y. Preparation of 2-Amino-4-

phenyl-4,5-dihydro-5*H*-1,3-thiazine Derivatives and Related Compounds for Treatment of Alzheimer's Disease. WO 2008133273 A1, November 6, 2008.

(32) Ellard, J. M.; Farthing, C. N.; Hall, A. Preparation of Fused Aminodihydrooxazine Derivatives as β-Amyloid Inhibitors and Useful in the Treatment of Neurodegenerative Disease Caused by Aβ in Particular Alzheimer-type Dementia. WO2011009898 A1, January 27, 2011.

(33) Robak, M. T.; Herbage, M. A.; Ellman, J. A. Synthesis and applications of *tert*-butanesulfinamide. *Chem. Rev.* **2010**, *110*, 3600–3740.

(34) Haveaux, B.; Dekoker, A.; Rens, M.; Sidani, A. R.; Toye, J.; Ghosez, L. α-Chloro enamines, reactive intermediates for synthesis: 1-chloro-*N*,*N*,2-trimethylpropenylamine. *Org. Synth.* **1980**, *59*, 26–34.

(35) Thaisrivongs, D. A.; Morris, W. J.; Tan, L.; Song, Z. J.; Lyons, T. W.; Waldman, J. H.; Naber, J. R.; Chen, W.; Chen, L.; Zhang, B.; Yang, J. A Next generation synthesis of BACE1 inhibitor verubecestat (MK-8931) *Org. Lett.* **2018**, *20*, 1568–1571.

Table of Contents Graphic: